Characteristics Assessment and Comparative Study of a Segmented-Stator Permanent-Magnet Hybrid-Excitation SRM Drive With High-Torque Capability

Wen Ding, *Member, IEEE*, Haigang Fu, and Yanfang Hu

***Abstract*—Hybrid-excitation switched reluctance motors (HESRMs) have attracted considerable attention for various drive applications due to their simple structure, low cost, and high-torque/power capabilities. This paper comprehensively evaluates and compares a high-torque segmented-stator HESRM drive with a conventional SRM drive in terms of static magnetic and dynamic performances. The stator of the segmented HESRM consists of six individual U-shaped segments; each one has two teeth associated with a permanent magnet (PM) installed between them. The static magnetic characteristics of a segmented HESRM and a conventional SRM, including flux distribution, phase flux linkage, electromagnetic torque, are analyzed and compared. The total fluxes created by the PM and by the excited current are strongly coupled. The details of mathematical model as well as dynamic performances of the segmented HESRM is derived and compared with the conventional SRM. Finally, a segmented HESRM and a conventional SRM of the same size are prototyped for experimental verification. From the comparative study, it is indicated that the segmented HESRM has better characteristics than the conventional SRM, such as less iron consumption, higher static and dynamic average torque production, lower torque ripple, higher power and torque densities, higher efficiency, and stronger starting capability. The measured results of static magnetic characteristic, steady-state and transient performances, and torque–speed characteristic of two SRM drives verify the finite-element analysis, modeling, and corresponding predictions.**

***Index Terms*—Dynamic performance, hybrid excitation, magnetic characteristic, permanent magnet (PM), segmented stator, switched reluctance motor (SRM).**

I. Introduction

In RECENT years, switched reluctance motors (SRMs) are experiencing widespread interest and increasingly employed in many industrial applications owing to its simple structure, high starting torque, low manufacturing cost, fault tolerance, and wide speed range in constant power operation [1]–[8]. However, it also suffers from some disadvantages, such as low torque and power densities, high-torque ripple, and acoustic noise when compared to other permanent magnet (PM) machines.

In order to improve some performances of SRMs, especially for lighter weight and higher power/torque density, many unique modular structures have been proposed in SRMs. Generally, they can be classified into two main categories which are termed as segmented-stator and segmented-rotor topologies. The segmented-stator topology is mainly divided into two groups: C-core and E-core configurations. In [9], a novel four-phase modular SRM with eight C-core stators is presented for low-cost production. It has better characteristics, such as higher torque and higher efficiency. In [10], a novel segmented SRM with C-shaped modules is proposed for wind power generation, which is easier to be started due to the lower weight. In [11] and [12], a segmented SRM with C-shaped stator cores is proposed for fault-tolerant drive systems. The iron loss is also lower than that of the conventional SRM. In [13], a novel five-phase pancake-shaped SRM with modular stator cores is designed and prototyped. It is shown that this novel SRM is able to improve the efficiency. In [14] and [15], a novel two-phase modular stator SRM with E-shaped cores is analyzed, optimized, prototyped, and experimentally tested. It is shown that this new type of E-core SRMs has 20% cost savings on copper, 20% steel savings, lower core losses, and higher average torque than the conventional SRM. Meanwhile, several novel types of segmented-rotor SRMs were proposed. In [16] and [17], the general application of segmented-rotor SRMs was first introduced by Mecrow. After that a segmented-rotor SRM with a greater number of rotor segments than stator slots is optimized in [18]. The effect of stator slot/rotor segment combination and number of phases on the performance of segmented rotor SRM is investigated in [19]. Novel two segmental-rotor SRMs with 6/5 pole and 12/8 pole are analyzed and experimented in [20] and [21], which have high efficiency. In [22], two types of 8/6 segmental-rotor SRMs with fully pitched windings and toroidal windings are proposed to provide lower losses and higher efficiency. In [23], a design process of optimizing an 80-kW segmental-rotor SRM to maximize efficiency for EVs is described. In [24] and [25], a novel

Manuscript received August 21, 2016; revised December 2, 2016; accepted January 30, 2017. Date of publication February 6, 2017; date of current version October 6, 2017. This work was supported by the National Natural Science Foundation of China under Grant 51477130. Recommended for publication by Associate Editor W. Qiao.

The authors are with the State Key Laboratory of Electrical Insulation and Power Equipment, School of Electrical Engineering, Xi'an Jiaotong University, Xi'an 710049, China (e-mail: dingwen_1981@163.com; dingwen_1981@stu.xjtu.edu.cn; stiwen@163.com).

Color versions of one or more of the figures in this paper are available online at http://ieeexplore.ieee.org.

Digital Object Identifier 10.1109/TPEL.2017.2665118

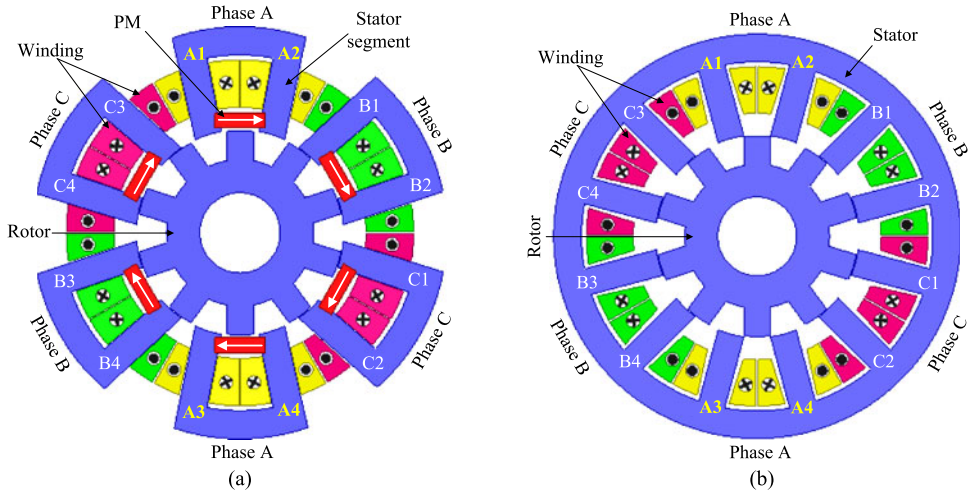

Fig. 1. Machine topologies of (a) 12/10-pole segmented-stator PM HESRM and (b) 12/10-pole conventional SRM.

modular SRM with six E-core stators and three segmented rotors is proposed. It is shown that this novel SRM has better characteristics, such as higher output torque and power density than classical SRM.

On the other hand, in order to further enhance the performance of SRMs, the concept of hybrid excitation with PMs was introduced into SRMs. In [26], a novel SRM that has auxiliary windings and PMs on stator yoke is presented. The torque is improved by auxiliary windings and PMs, and the efficiency is also improved 3%. In [27] and [28], a supermultipolar PM switched reluctance generator is proposed for small-scale wind-turbine generation. In [29]–[31], a novel single-phase hybrid switched reluctance motor which has four stator reluctance poles and two stator PM poles is proposed for pump drive system. In [32], a novel 6-/5-pole three-phase HRM is studied. It is shown that this HRM has shorter magnetic circuits, lower iron losses, higher efficiency, and power density than the conventional SRM. In [33] and [34], a variety of HRMs with different stator/rotor pole pairs are also proposed to improve output torque, efficiency, and power density. Furthermore, the authors previously presented and preliminarily analyzed a segmented-stator hybrid-excitation SRM (HESRM) with PMs for EVs in EVER2016 [35]. However, the comparative studies on the static magnetic characteristic, modeling, dynamic and transient performances as well as experimental verification between the segmented-stator HESRM and conventional SRM have not been performed in that literature.

The main purpose and novelty of this paper are to extend the conference paper [35] and concern on comprehensive evaluation of the machine performances and comparative study of a 12/10 segmented-stator HESRM drive and a 12/10 conventional SRM drive. The static magnetic characteristics, mathematical models, and dynamic and transient performances of two SRM drives are compared and validated. This paper is organized as follows. Section II gives the basic machine topologies. Section III compares the static magnetic characteristics of a segmented HESRM with a conventional SRM, including flux distribution, phase flux linkage, electromagnetic torque, etc. After that the details of

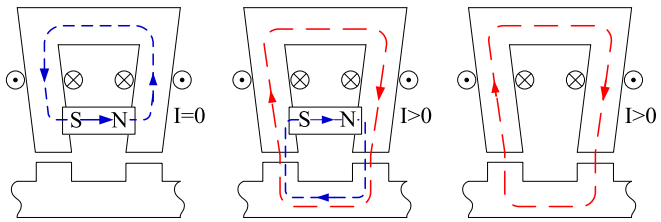

Fig. 2. Magnetic circuits of the segmented HESRM when the coils are (a) not excited and (b) excited. (c) Magnetic circuit of a modular electromagnet when the coils are excited.

mathematical models and dynamic and transient performances are presented and compared in Section IV. The investigated segmented HESRM and conventional SRM with the same size are prototyped and developed for validation in Section V. Finally, some conclusions are drawn in Section VI.

II. Machine Topologies of Two SRMs

The machine topologies of the investigated 12/10 segmented-stator PM HESRM and 12/10 conventional SRM are shown in Fig. 1. It can be seen that both two SRMs have the same rotor configuration which features ten salient poles and without any PMs or coils in it, but the stator topologies in these two machines are different.

First, the stator of segmented HESRM consists of six individual U-shaped electrical steel laminated segments. Each one has two teeth and the concentrate armature winding coils are wound on the teeth. There is a PM installed between two poles in each stator segment. Second, it can be observed that there is neither yoke iron nor other ferromagnetic material between two adjacent U-shaped segments in the segmented HESRM. The six U-shaped segments are evenly arranged along the rotor, which are characterized by their own independent magnetic structures. The 12 coils which are twisted on the stator poles make up three phases indicated as A, B, and C.

Fig. 2(a) shows the magnetic circuit in one segment of the HESRM when none of the coils is excited at aligned position.

TABLE I
MAIN PARAMETERS AND SPECIFICATIONS OF TWO SRMS

Parameters	Segmented-Stator HESRM	Conventional SRM
Phase number	3	3
Stator and rotor poles	12/10	12/10
Rated power (W)	600	500
Rated speed (r/min)	1000	1000
Maximum speed (r/min)	2000	2000
Rated torque (N·m)	6.0	5.0
Stator outer diameter (mm)	124	124
Stator- and rotor-pole arcs (°)	15/15	15/15
Stator yoke width (mm)	8.5	8.5
Rotor yoke width (mm)	10	10
Axial length (mm)	63	63
Air-gap length (mm)	0.3	0.3
Number of coil turns per pole	80	80
Winding weight (kg)	1.424	1.424
Stator iron weight (kg)	1.952	2.558
Rotor iron weight (kg)	0.858	0.858
Type of PMs and weight (kg)	NdFeB30/0.191	–
Total effective machine weight (kg)	4.425	4.840
Electric steel material	DW470	DW470

It can be seen that the flux generated by the PM is only closed through the U-shaped segment and does not cross rotor core and air gap. When the coils are excited with a current, the magnetic circuit of one segment at the same position is shown in Fig. 2(b). The dot and cross symbols indicate the directions of phase winding currents. The red arrows indicate the flux generated by phase winding currents and the blue arrows indicate the magnetic flux generated by PMs. It can be observed that the flux produced by excited coils and the flux produced by the PM are added together. Both flux paths are in the same direction in the rotor tooth and air gap. Thus, the sum of magnetic fluxes will create a larger electromagnetic attraction force than that created by a normal electromagnet in conventional SRM. Accordingly, the magnetic circuit of a modular electromagnet when the coils are excited at aligned position is shown in Fig. 2(c).

III. MAGNETIC CHARACTERISTICS OF TWO SRMS

In this section, the comparison of static magnetic characteristics between a segmented HESRM and a conventional SRM is made by using the finite-element analysis (FEA). It should be noted that in order to ensure a fair comparison, both two SRMs have the same size, the same number of coils per pole, as well as the same winding configuration and connection. The main dimensions and specifications of these two SRMs are listed in Table I.

As can be seen from Fig. 1, the cross-sectional areas of two rotors are the same due to the same rotor construction and geometrical dimensions. Thus, both SRMs have the identical rotor iron weights, but the stator iron weights of two SRMs are different. First, because of the additional stator back iron in the conventional SRM and the modular-stator topology in the segmented HESRM, the stator iron weight of HESRM is lower than that of the conventional SRM by 31.1%. Owing to this difference, it will result in less electrical steel consumption compared to the conventional SRM with the same stator dimension.

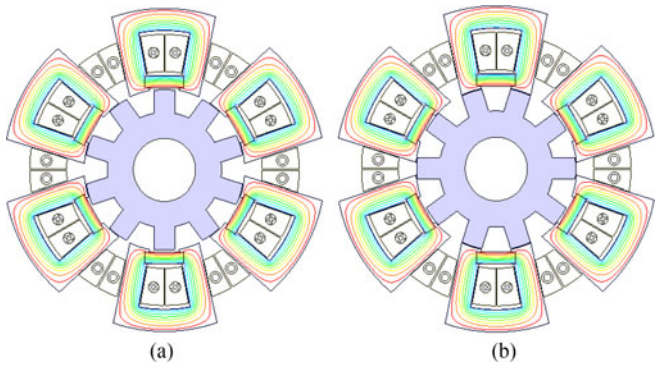

Fig. 3. Magnetic field distributions of the segmented HESRM by PMs only at (a) unaligned position and (b) aligned position.

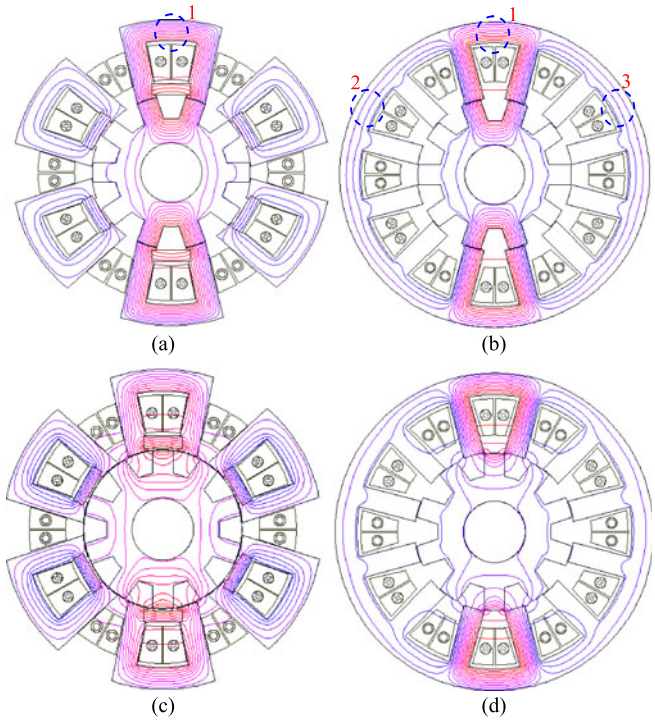

Fig. 4. Magnetic field distributions of two SRMs. (a) Segmented HESRM at aligned position. (b) Conventional SRM at aligned position. (c) Segmented HESRM at unaligned position. (d) Conventional SRM at unaligned position.

Finally, although the segmented HESRM has six PMs in the stator, the entire effective machine weight is lighter than that of the conventional SRM by 9.4%, which will result in potential higher torque density. However, it should be noted that owing to the rare earth PM NdFeB used in the segmented HESRM and it is more expensive than iron lamination, which offsets part of the saving of some iron lamination.

A. Field Line and Flux Distributions

Fig. 3 demonstrates the magnetic field distributions of the segmented HESRM due to the PMs only at unaligned and aligned positions. It can be observed that the flux produced by each PM is only closed through the U-shaped stator segment core and does not cross rotor and air gap. Fig. 4 compares magnetic field distributions of two SRMs when one phase (A) is excited with

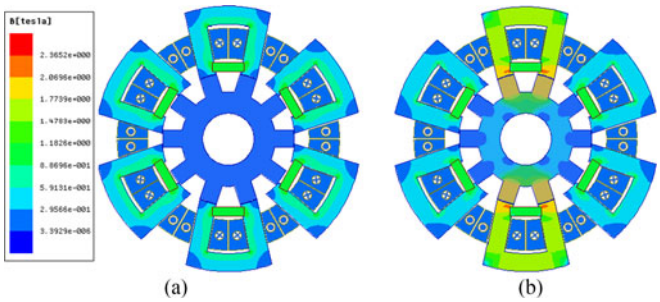

Fig. 5. Flux density distributions of the segmented HESRM when (a) all windings are not excited and (b) one phase is excited with 13 A at aligned position.

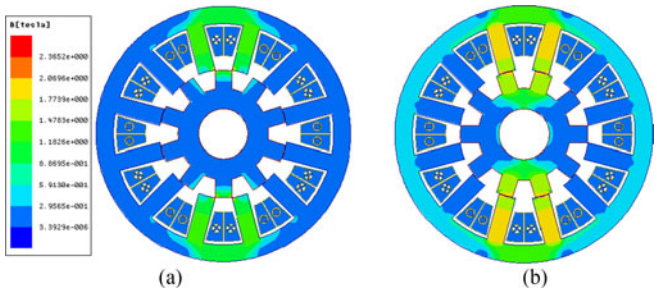

Fig. 6. Flux density distributions of the conventional SRM for a current of 13 A at (a) unaligned position and (b) aligned position.

the same current $i_{ph\mathrm{A}} = 13$ A. Apparently, there are a lot of differences between the magnetic field distributions of these two SRMs. First, it is clear that the main flux is only produced by the excited coils in conventional SRM, which crosses both the air gap and rotor. The flux in the stator back iron could be divided into three parts, as shown in the regions of 1, 2, and 3. Second, the fluxes produced by the excited coils and the PM are added together to cross the air gap and rotor in the HESRM. They are both closed through the segment core of excited stator phase and the PM. While the flux due to the PM, only in nonexcited phase, is only closed through the stator yoke and does not cross air gap.

Fig. 5 shows the flux density distributions of the HESRM when all windings are not excited and when one of phases is excited with the current $i_{ph\mathrm{A}} = 13$ A, respectively. It can be seen that when all windings are not excited, the maximum flux density due to the PM only in stator pole is approximately 1.18–1.47 T. When one phase is excited with the same current $i_{ph\mathrm{A}} = 13$ A, the maximum flux density in stator pole is about 2.06–2.36 T.

Fig. 6 shows the flux density distributions of the conventional SRM when one phase is excited with the current $i_{ph\mathrm{A}} = 13$ A. As can be seen from Figs. 5(b) and 6(b), when one phase (A) is excited with the same current $i_{ph\mathrm{A}} = 13$ A, the average flux density in stator pole of the HESRM is approximately 1.47–1.77 T. While in the same area of the conventional SRM, the average flux density is about 1.77–2.07 T, which means the machine begins to become saturated at this situation.

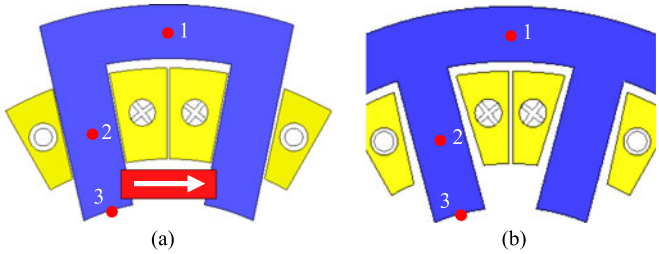

Fig. 7. Points in stator and air gap for comparison of flux density. (a) Segmented HESRM. (b) Conventional SRM.

In order to investigate the effect of phase current on saturation degree of two SRMs, the flux density distributions of three points in the stator and air gap are compared. The three points are located in the same positions of two SRMs and denoted by points 1, 2, and 3, as shown in Fig. 7. It should be noted that points 1 and 2 are located in the center of stator yoke and pole, and point 3 is located in the center of air gap between the stator pole and rotor pole. The points 1, 2, and 3 flux density distributions versus phase current at aligned position in two SRMs are compared in Fig. 8. As can be seen from Fig. 8(a) and (b), when the current is over 5 A, points 1 and 2 in the conventional SRM begin to become saturated. While the same point positions in the HESRM are not saturated with the same current. In addition, the flux density does not increase with the current increases in the HESRM. For example, at 2 A, the flux density in points 1 and 2 in the HESRM reaches the minimum. In addition, the air-gap flux density of the HESRM is a little higher than that of the conventional SRM from 4.5 to 25 A, as shown in Fig. 8(c).

From Fig. 2, it can be seen that the air-gap flux density of the HESRM appears to be higher than the conventional SRM, and the flux density in stator back iron and teeth appears to be lower. This is because in the air gap, the direction of flux from the PM is in the same with the flux from coils, but the directions in the stator back iron and teeth are opposite, as shown in Fig. 2(b). Therefore, the fluxes produced by excited coils and PM are added together in the air gap. While in the stator back iron and teeth, they offset some part of each other. However, it should be noted that in Fig. 2(c), the stator is a modular structure, not a conventional monolithic structure. Thus, the flux distribution of the conventional monolithic structure would be different from the modular structure, as shown in Fig. 4(b). In fact, as seen in Fig. 4, the flux distribution of the HESRM is indeed different from the conventional SRM. In Fig. 4(b), the flux in stator back iron of the conventional SRM could be divided into three parts, as shown in the regions of 1, 2, and 3. In this situation, the total flux in stator teeth is the sum of these three parts of magnetic fluxes. While in the HESRM, the flux in stator back iron is the same with that in stator teeth, as shown in Fig. 4(a). Thus, the flux density in stator back iron of the conventional SRM might be lower than that in the same region of the HESRM. The results shown in Fig. 8 are corresponding to the above comments. For example, Figs. 5(b), 6(b), and 8(a) illustrate that the flux density in stator back iron of the HESRM is higher than

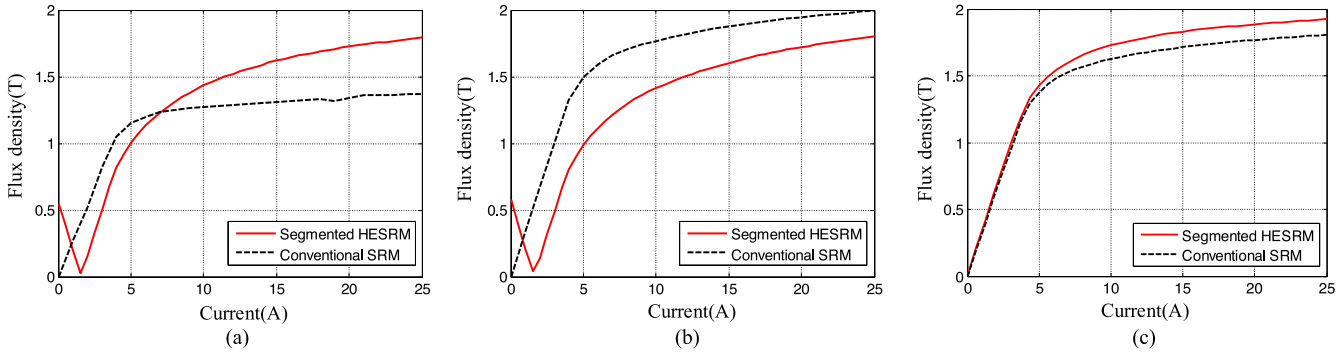

Fig. 8. Comparison of flux density distributions in the stator and air gap versus phase current in two SRMs. (a) Point 1. (b) Point 2. (c) Point 3.

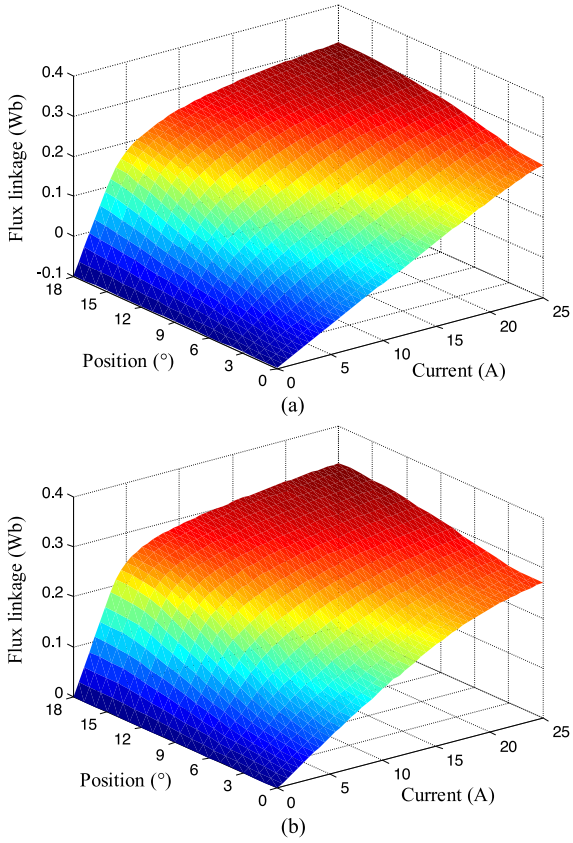

Fig. 9. Static phase flux linkage characteristics of the (a) segmented HESRM and (b) conventional SRM.

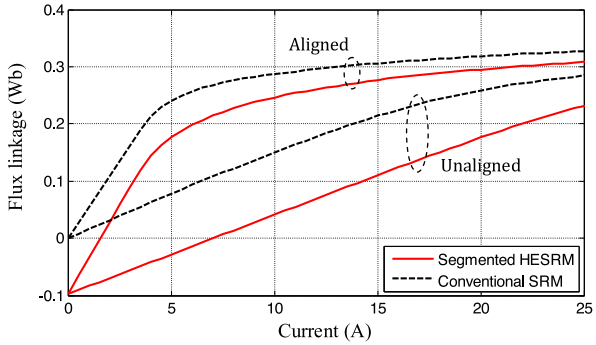

Fig. 10. Comparison of phase flux linkage characteristics for two SRMs at different rotor positions.

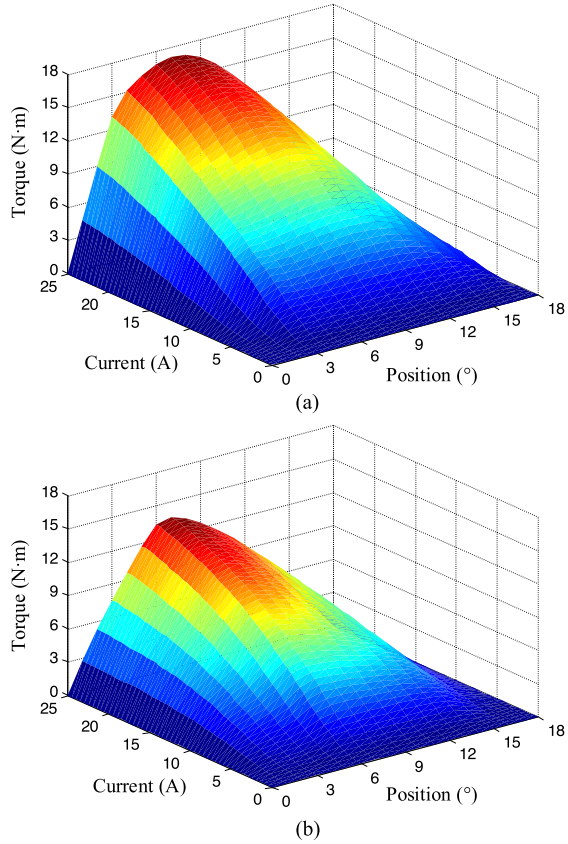

Fig. 11. Static torque characteristics of the (a) segmented HESRM and (b) conventional SRM.

that in the same region of the conventional SRM. Figs. 5(b), 6(b), and 8(b) illustrate that the flux density in the stator teeth of the HESRM is lower than that in the same region of the conventional SRM. Fig. 8(c) illustrates that the flux density in the air gap of the HESRM is higher than that in the same region of the conventional SRM. Thus, to some extent, the HESRM might produce more torque than the conventional SRM.

B. Static Phase Flux Linkage

Fig. 9 shows 3-D flux linkage characteristics of two SRMs for different phase currents from unaligned position to aligned position. Additionally, the phase flux linkage curves of two

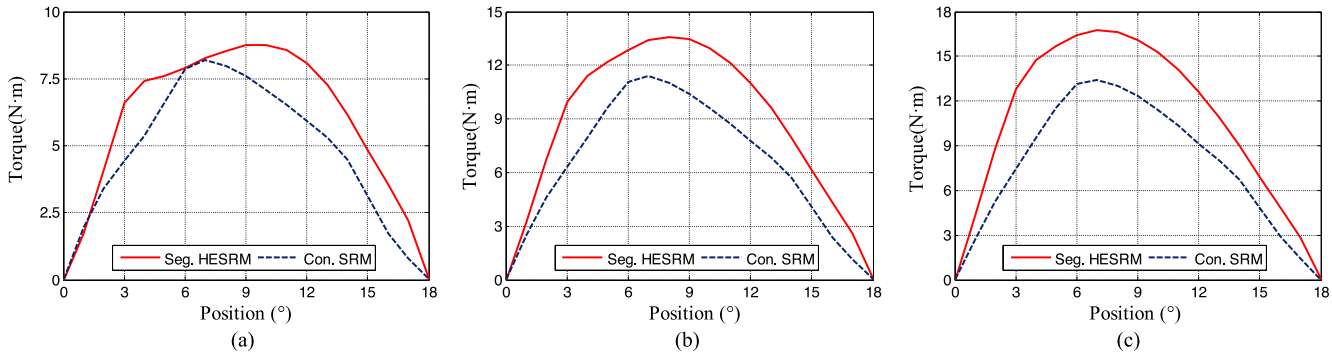

Fig. 12. Comparison of static torque curves for two SRMs with three current levels. (a) 12 A. (b) 18 A. (c) 24 A.

TABLE II
COMPARISON OF STATIC AVERAGE TORQUE FOR DIFFERENT CURRENTS

Current	5 A	8 A	12 A	15 A	18 A	24 A
Segmented HESRM, Torque, N·m	1.76	3.65	6.05	7.63	8.97	10.9
Conventional SRM, Torque, N·m	1.70	3.16	4.84	5.85	6.65	7.86
Percentage Difference in Their Torques	3.52%	15.5%	25.0%	30.4%	34.9%	38.7%

SRMs with two typical positions are compared, as shown in Fig. 10. As can be seen from these figures, when the current in winding coils is 0 A, there is no phase flux linkage produced in the conventional SRM, while the phase flux linkage due to the PM only in the HESRM is −0.1 Wb at this situation. It can also be noticed that the phase flux linkage of the HESRM is lower than that of the conventional SRM with the same phase current. In other words, this means that the conventional SRM is more likely to become saturated than the HESRM with the same current. As is well known, in an SRM, the area enclosed between the aligned and unaligned curves of the flux linkage with the fixed current is the change in coenergy, which corresponds to the energy converted to torque in a single stroke [36]. As can be seen from Fig. 10, it is evident that the enclosed area of the flux linkage for the HESRM is larger than that for the conventional SRM at a fixed current from unaligned to aligned positions, especially among large current range. It means that the average torque of the HESRM with a fixed current is larger than that of the conventional SRM.

C. Static Electromagnetic Torque

The static magnetic torque characteristics of two SRMs with one phase excitation are shown in Fig. 11. Three static torque curves of two SRMs with the current levels of 12, 18, and 24 A are compared in Fig. 12. Accordingly, the average torque for one half of excitation cycle with several current levels is calculated and shown in Table II. From the comparison, it can be seen that higher static torque is obtained in the HESRM, especially among the large current range, and the superiority becomes larger and larger with the current increases. For example, the HESRM produces 25% and 38.7% larger torques than the conventional SRM at 12 and 24 A. The maximum torque of the HESRM is also larger than that of the conventional SRM with the same excitation current. In other words, the coil current requirement of the HESRM is less than the conventional SRM for the same torque production.

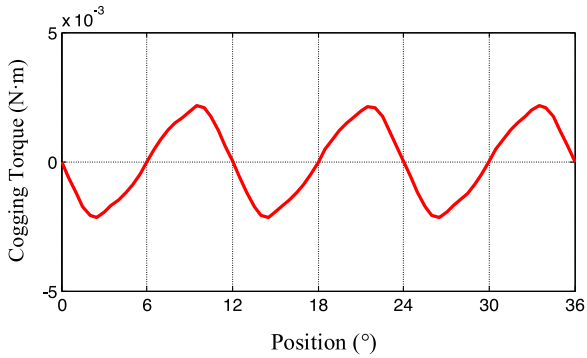

Fig. 13. Cogging torque versus position (without current in the coils) in the segmented HESRM.

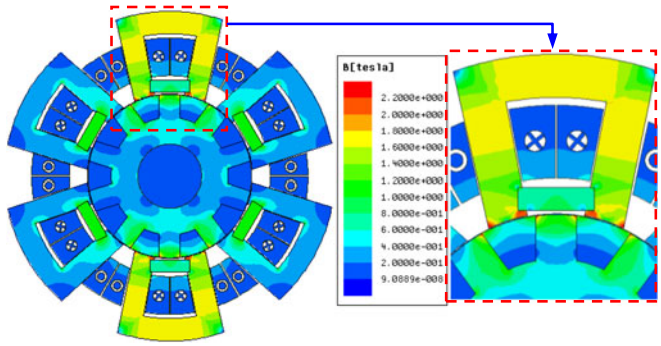

Fig. 14. Flux density distribution of the HESRM when one phase winding is excited with a rather high current of 30 A.

Apart from the static magnetic characteristics, the cogging torque is also an important optimal objective in PM motor designs. The cogging torque is usually caused by the interaction between rotor poles and PMs versus rotor position when the coils are not excited. It is an undesired effect for a PM motor under dynamic operation. The cogging torque in the HESRM is shown in Fig. 13. It can be observed that the peak-to-peak value of the cogging torque is about −0.002 to 0.002 N·m, which is nearly zero. The main reason for this is that there is almost no flux that passes the rotor and air gap when the windings are not

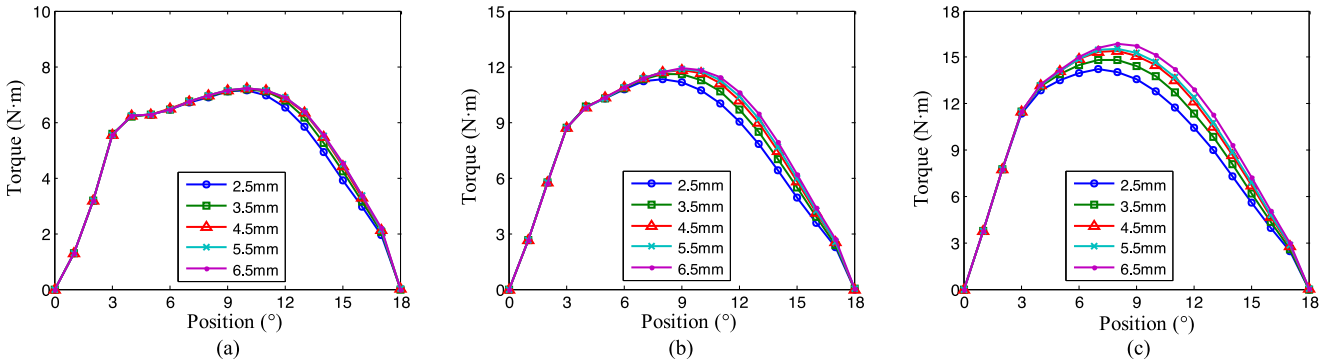

Fig. 15. Static torque curves of the segmented HESRM with different PM thicknesses for different current levels. (a) 10 A. (b) 15 A. (c) 20 A.

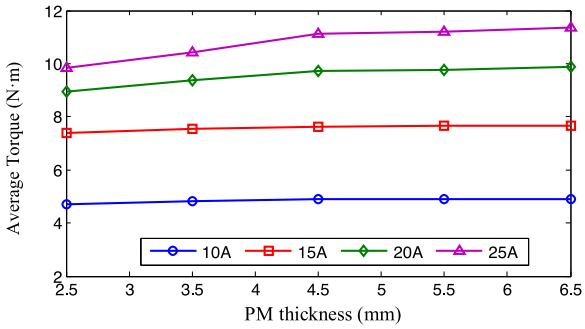

Fig. 16. Influence of PM thickness on static average torque.

TABLE III
MAIN PARAMETERS AND SPECIFICATIONS OF THE SEGMENTED SRM

Parameters	Values	Parameters	Values
Phase number	3	Air-gap length (mm)	0.3
Stator and rotor poles	12/10	Number of coil turns per pole	80
Stator outer diameter (mm)	124	Winding weight (kg)	1.424
Stator- and rotor-pole arcs (°)	15/15	Stator iron weight (kg)	2.010
Stator yoke width (mm)	8.5	Rotor iron weight (kg)	0.858
Rotor yoke width (mm)	10	Total effective machine weight (kg)	4.292
Axial length (mm)	63	Electric steel material	DW470

excited, which may be the most obvious merit over other types of PM motors.

Furthermore, the existence of PM means that there is a need to study the demagnetization. When one phase winding is excited with a rather high current of 30 A at the unaligned position, the flux density distribution of the HESRM is shown in Fig. 14. It should be noted that for the HESRM when it is working, the phase current is normally lower than 20 A. It can be seen from Fig. 14 that the flux density in the PM is about 0.6–1.2 T, which is much higher than 0.4 T; thus, the PM NdFeB will not be demagnetized irreversibly under this excitation condition [37]. On the other hand, the slot space factor of the HESRM is about 45%, there is enough space for the windings and PMs to cool.

D. Influence of PM Thickness

To evaluate the influence of the PM on torque production in the HESRM, a sensitivity analysis of the static torque production based on PM thickness is performed. Fig. 15 shows the static torque curves from unaligned to aligned positions obtained with different PM thicknesses. Accordingly, the values of average torque with different PM thicknesses are shown in Fig. 16. As shown in these figures, although the static torque increases with the increase of PM thickness, the higher PM thickness will leave less space for the coils, and besides, the low-cost advantage of the HESRM in relation to other PM machines is reduced. Hence, a balance must be considered between the PM thickness and space for the coils during optimization of a machine design. According to all of the above analysis and comments, the PM thickness is selected to 4.5 mm in this paper.

E. Comparison With Segmented SRM

From above analysis, since the entire back iron is not used in the segmented HESRM, then the 12/10 conventional SRM can be also segmented. In order to evaluate the performance of this segmented SRM, all the dimensions, parameters, and number of turns are the same with the conventional SRM, as shown in Table III. The machine topology, flux distribution, and electromagnetic torque of the 12/10 segmented SRM and a comparison with other two motors are shown in Figs. 17–19. As shown in the tables and figures, the stator of 12/10 conventional SRM is heavier than that of the segmented SRM. The segmented HESRM has the largest torque among the three motors and the conventional SRM produces higher torque than the segmented SRM at the same current. Highest static average torque is obtained with the segmented HESRM in large current range and the superiority becomes larger and larger with the current increases. The conventional SRM produce higher average torque than the segmented SRM. In a word, although the segmented SRM has lower weight than the conventional SRM, the electromagnetic torque performance appears to be worse than the conventional SRM.

IV. MATHEMATIC MODEL AND DYNAMIC PERFORMANCE COMPARISON

A. Mathematical Model of Segmented HESRM

According to above analysis, when the HESRM is working, the flux in the excited phase-x is composed of two parts which

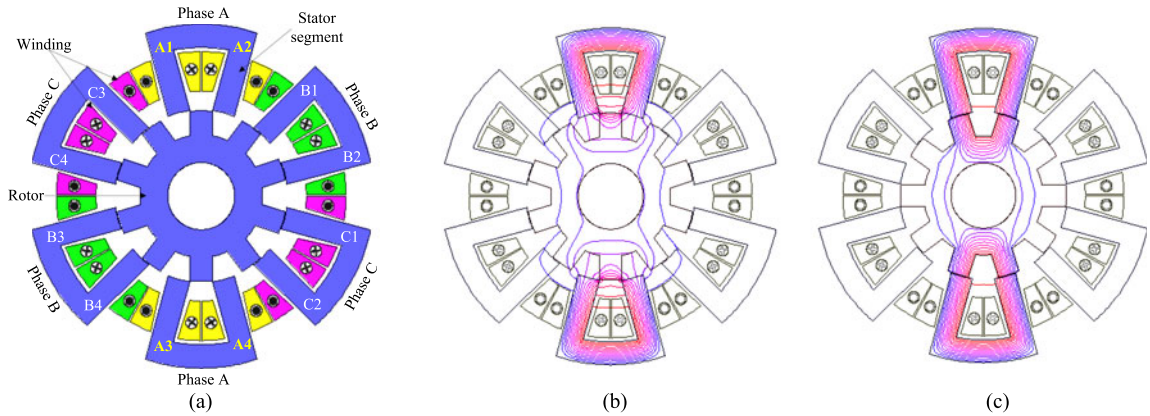

Fig. 17. (a) Machine topology of 12/10 segmented SRM. Magnetic field distributions at (b) unaligned position and (c) aligned position.

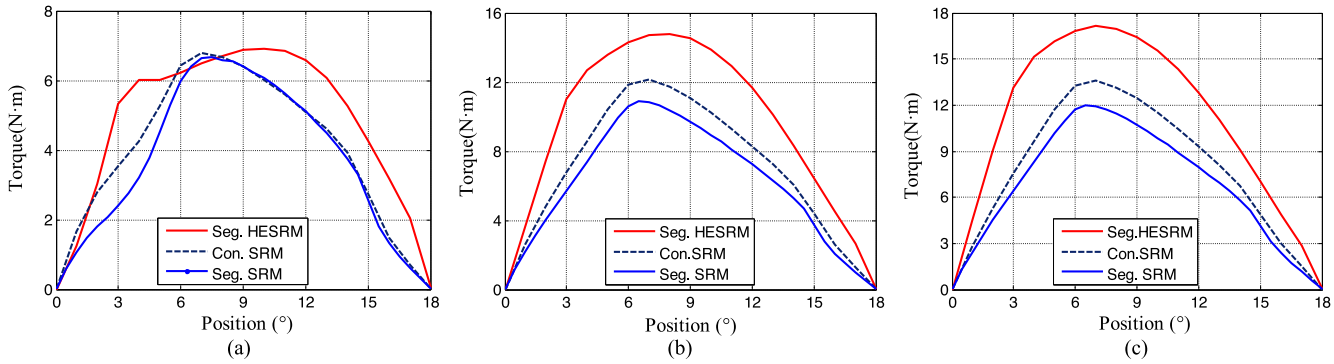

Fig. 18. Comparison of static torque curves in three SRMs with different current levels. (a) 10 A. (b) 20 A. (c) 25 A.

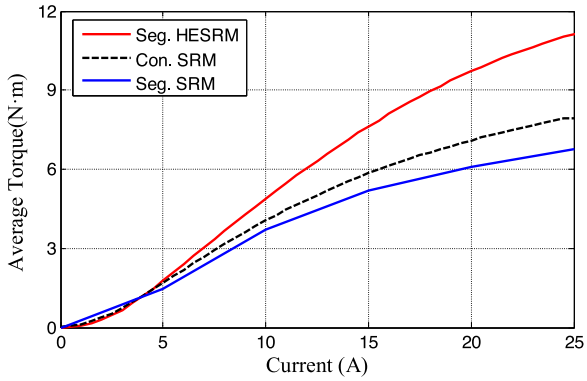

Fig. 19. Comparison of static average torque characteristics in three SRMs.

are produced by PM and excited phase coils, respectively. It also means that the phase total flux linkage is the sum of the flux linkages created by PM and by excited phase coils as follows:

$$\psi_x = \psi_{ix}(\theta, i_x) + \psi_{pmx}(\theta, i_x) \tag{1}$$

where ψ_x is the total flux linkage in excited phase, $\psi_{ix}(\theta, i_x)$ is the flux linkage created by excited current, and $\psi_{pmx}(\theta,\ i_x)$ is the flux linkage created by PM, θ is the rotor position.

Generally, the flux linkage due to the excited current is expressed as the product of inductance and current; thus, the phase flux linkage in the excited phase can be rewritten as

$$\psi_x = \psi_{ix}(\theta, i_x) + \psi_{pmx}(\theta, i_x) = L_{ix}(i_x, \theta) \cdot i_x + \psi_{pmx}(\theta, i_x) \tag{2}$$

where $L_{ix}(\theta,\ i_x)$ is the inductance created by the excited current and is also a function of the phase current and rotor position.

The voltage equation of the excited phase-x can be expressed as

$$\frac{d\psi_x}{dt} = u_x - r_{ph} \cdot i_x \tag{3}$$

where u_x, r_{ph}, i_x, and ψ_x are the phase voltage, phase resistance, phase current, and phase flux linkage.

Substituting (2) into (3), the phase voltage equation of the excited phase can be described as

$$u_x = r_{ph} \cdot i_x + L_{ix}(i_x, \theta) \cdot \frac{di_x}{dt} + \omega \cdot i_x \cdot \frac{dL_{ix}(i_x, \theta)}{d\theta} + \omega \cdot \frac{d\psi_{pmx}(\theta, i_x)}{d\theta}. \tag{4}$$

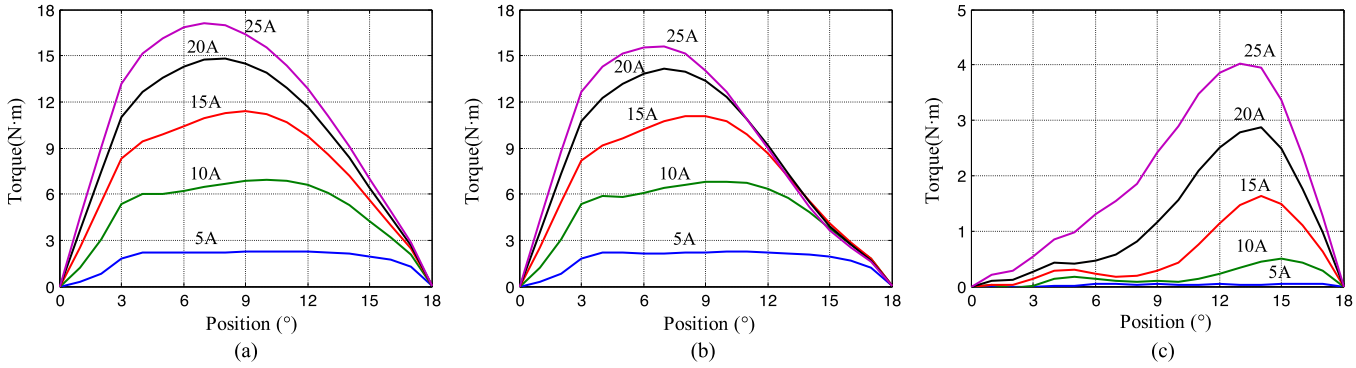

Fig. 20. Static torque profiles of (a) total torque, (b) reluctance torque, and (c) PM torque with several current levels in the HESRM.

Then, the whole phase voltage equations for a three-phase segmented HESRM can be expressed as

$$\begin{bmatrix} u_A \\ u_B \\ u_C \end{bmatrix} = r_{ph} \cdot \begin{bmatrix} i_A \\ i_B \\ i_C \end{bmatrix} + \begin{bmatrix} L_{iA} & 0 & 0 \\ 0 & L_{iB} & 0 \\ 0 & 0 & L_{iC} \end{bmatrix} \cdot \begin{bmatrix} \dfrac{di_A}{dt} \\ \dfrac{di_B}{dt} \\ \dfrac{di_C}{dt} \end{bmatrix} + \omega \cdot \begin{bmatrix} i_A & 0 & 0 \\ 0 & i_B & 0 \\ 0 & 0 & i_C \end{bmatrix} \cdot \begin{bmatrix} \dfrac{dL_{iA}}{d\theta} \\ \dfrac{dL_{iB}}{d\theta} \\ \dfrac{dL_{iC}}{d\theta} \end{bmatrix} + \omega \cdot \begin{bmatrix} \dfrac{d\psi_{pmA}}{d\theta} \\ \dfrac{d\psi_{pmB}}{d\theta} \\ \dfrac{d\psi_{pmC}}{d\theta} \end{bmatrix}. \tag{5}$$

The total coenergy W_x in the excited phase is obtained as

$$W_x = W_{ix}(\theta, i_x) + W_{pmx}(\theta, i_x) \tag{6}$$

where $W_{ix}(\theta, i_x)$ is the coenergy developed by the excited current, and $W_{pmx}(\theta)$ is the coenergy developed by the PM.

The electromagnetic torque T_x produced by one phase can be derived from the total coenergy of that phase as

$$\begin{aligned} T_x(\theta, i_x) &= \frac{\partial W_{ix}(\theta, i_x)}{\partial \theta}|_{i_x=\text{const}} + \frac{\partial W_{pmx}(\theta, i_x)}{\partial \theta} \\ &= T_{rx}(\theta, i_x) + T_{pmx}(\theta, i_x) \end{aligned} \tag{7}$$

where T_{rx} is the electromagnetic torque developed by excited current which is called reluctance torque and T_{pmx} is the electromagnetic torque developed by PMs in the excited phase which is called PM torque.

By inspection of (1)–(7), it can be observed that the total flux linkage, coenergy, and electromagnetic torque for the excited phase in the HESRM are summations of two distinctive parts. However, owing to the motor's inherent magnetic saturation under load conditions, it makes $\psi_{cx}(\theta, i)$ and $\psi_{pmx}(\theta, i)$, T_{rx} and T_{pmx} highly dependent on the phase current. Thus, the above two group of variables are normally strongly coupled.

In order to decouple the torque from the PM and from reluctance in the HESRM, the static PM torque and reluctance torque

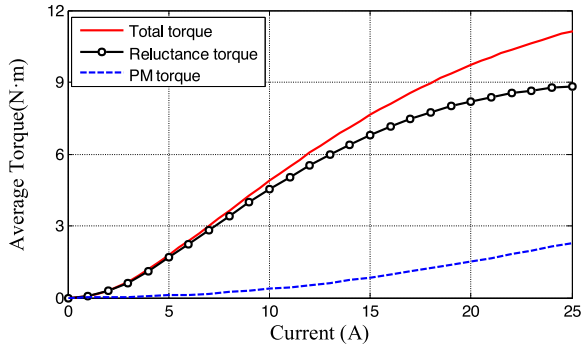

Fig. 21. Comparison of static average torque profiles for three types of torque in the HESRM.

TABLE IV
COMPARISON OF STATIC AVERAGE TORQUE FOR THREE TYPES OF TORQUE

Current	5 A	10 A	15 A	20 A	25 A
Total torque, N·m	1.76	4.88	7.63	9.72	11.1
Reluctance torque, N·m	1.67	4.51	6.77	8.20	8.83
	94.9%	92.4%	88.7%	84.4%	79.5%
PM torque, N·m	0.09	0.37	0.86	1.52	2.27
	5.1%	7.6%	11.3%	15.6%	20.5%

characteristics are calculated from FEA, which are illustrated in Fig. 20. Accordingly, the average torque profiles and values for three types of torque in the HESRM for one half of excitation cycle with several current levels is calculated and shown in Fig. 21 and Table IV. As shown in these figures and table, the reluctance torque is much higher than the PM torque when one phase is excited. For example, the percentage of torque from the PM and from reluctance is 92.4% and 7.6% at 10 A and 79.5% and 20.5% at 25 A, respectively. Thus, it may be said that the reluctance torque is dominant in the HESRM, but the PM torque becomes larger and larger with the current increases.

B. Dynamic Performance of Two SRM Drives

MATLAB/Simulink is used to perform the simulation of two SRM drives. The Simulink model of the HESRM drive system consists of the machine model, speed controller, asymmetric

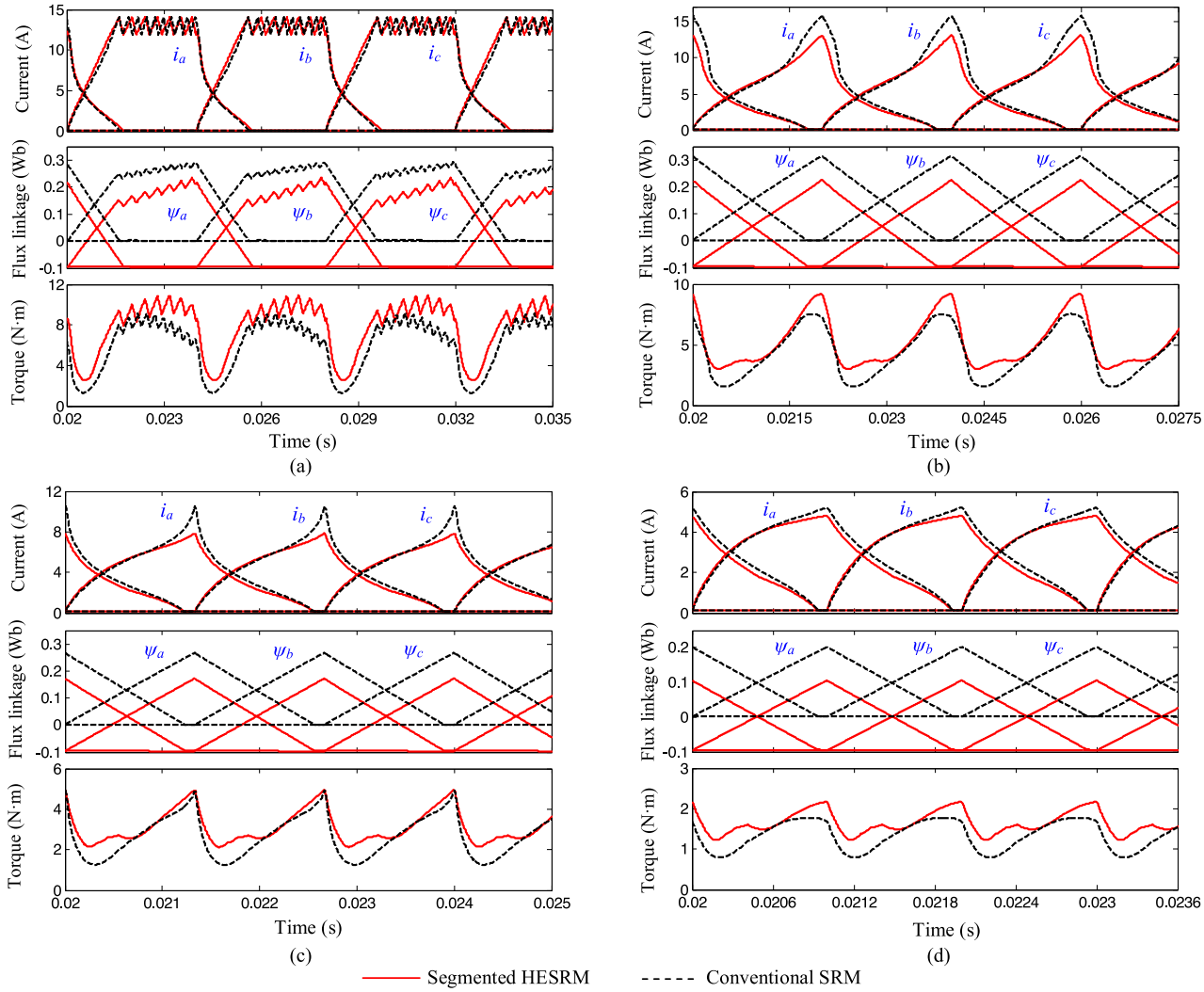

Fig. 22. Comparisons of a steady-state performance of two SRMs with (a) CCC mode at 500 r/min, (b) APC mode at 1000 r/min, (c) APC mode at 1500 r/min, and (d) APC mode at 2000 r/min.

half-bridge power converter, logic PWM, angle controller, mechanical system and dc source, etc. It should be noted that the machine model mainly concludes flux linkage and torque characteristics.

The dynamic performances of two SRMs under the same conditions are performed and compared, which are conducted with current chopping control (CCC) for a low speed of 500 r/min and angle position control (APC) for a medium speed of 1000 r/min and two high speeds of 1500 and 2000 r/min, respectively. Fig. 22 compares the simulated waveforms of two SRMs operation with CCC mode and APC mode under the same voltage and different speed conditions. Table V gives detailed summary of the predicted performances in two SRMs.

As shown in Fig. 22 and Table V, the HESRM seems to have better dynamic characteristics than the conventional SRM. At the low speed, the phase current of HESRM is almost the same with the conventional SRM due to the hysteresis control, but the maximum and average torque values of the former are larger than those of the latter. With the single-pulse control at high speeds, as shown in Fig. 22(b)–(d), the phase current of HESRM is lower than that of the conventional SRM, while the average torque of the former is larger than that of the latter and the torque ripple

TABLE V
SUMMARY OF PREDICTED DYNAMIC PERFORMANCES OF TWO SRMS

	Segmented HESRM				Conventional SRM			
Control modes	CCC		APC		CCC		APC	
Speed, r/min	500	1000	1500	2000	500	1000	1500	2000
DC-link voltage, V	170	170	210	210	170	170	210	210
RMS phase current, A	6.82	5.08	3.60	2.55	6.84	5.81	3.94	2.68
Average torque, N·m	7.88	5.26	3.23	1.66	6.07	4.26	2.68	1.36
Torque per Ampere, N·m/A	1.16	1.04	0.90	0.65	0.89	0.73	0.68	0.51
Torque ripple, %	105.9	117.8	89.2	57.2	122.9	131.0	134.8	72.8
Torque density, N·m/kg	1.78	1.19	0.73	0.38	1.25	0.88	0.55	0.28
Output power, W	412.4	550.5	507.1	347.5	317.6	445.9	420.7	284.7
Output power density, W/kg	93.2	124.4	114.6	78.5	65.6	92.1	86.9	58.8
Copper loss, W	167.4	92.9	42.7	23.4	168.4	121.5	55.9	25.9
Copper loss per torque, W/N·m	21.2	17.7	13.2	14.1	27.7	28.5	20.9	19.0

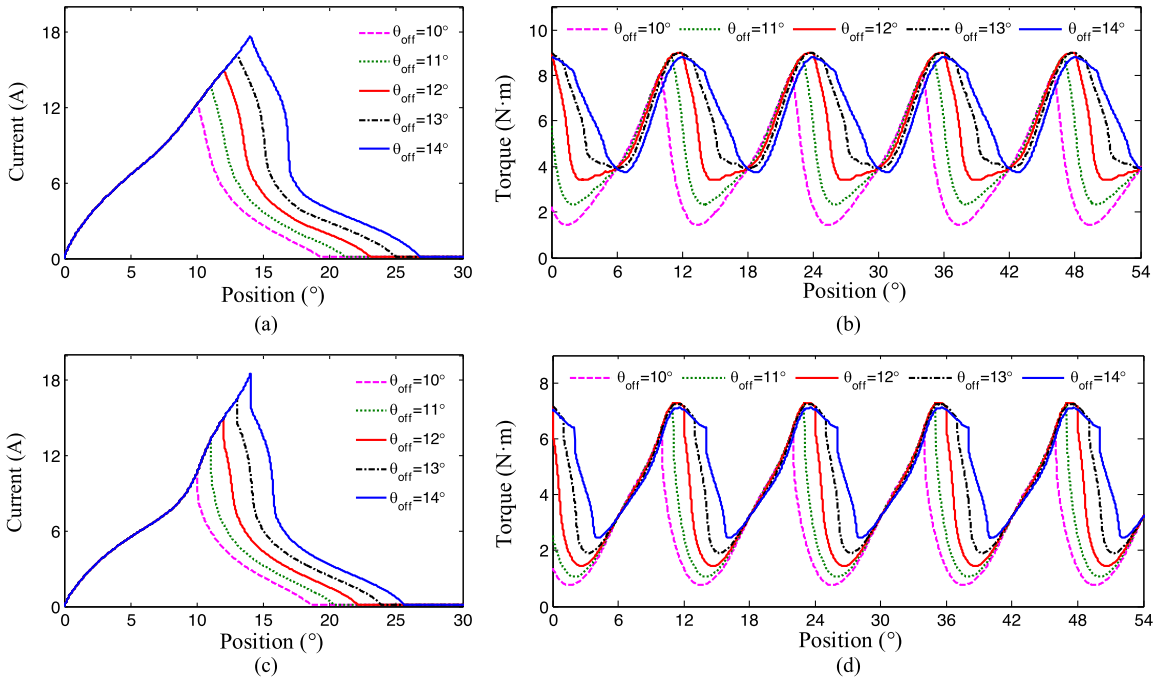

Fig. 23. Phase current and torque waveforms of two SRMs obtained by varying turn-off angles at $\theta_{on} = 0°$. (a) and (b) Segmented HESRM. (c) and (d) Conventional SRM.

TABLE VI
DYNAMIC PERFORMANCE OF THE HESRM WITH DIFFERENT TURN-OFF ANGLES AT $\theta_{on} = 0°$

Parameter	$\theta_{on} = 0°$				
	$\theta_{off} = 10°$	$\theta_{off} = 11°$	$\theta_{off} = 12°$	$\theta_{off} = 13°$	$\theta_{off} = 14°$
RMS phase current, A	4.50	5.17	5.85	6.74	7.70
Average torque, N·m	3.84	4.74	5.53	6.09	6.27
Torque per Ampere, N·m/A	0.85	0.92	0.94	0.90	0.82
Torque ripple	174.9%	137.4%	101.3%	83.8%	81.0%

TABLE VII
DYNAMIC PERFORMANCE OF THE HESRM WITH DIFFERENT TURN-OFF ANGLES AT $\theta_{on} = 1°$

Parameter	$\theta_{on} = 1°$				
	$\theta_{off} = 10°$	$\theta_{off} = 11°$	$\theta_{off} = 12°$	$\theta_{off} = 13°$	$\theta_{off} = 14°$
RMS phase current, A	3.48	4.04	4.72	5.51	6.42
Average torque, N·m	2.55	3.29	4.05	4.66	4.98
Torque per Ampere, N·m/A	0.73	0.82	0.86	0.84	0.78
Torque ripple	202.6%	176.1%	141.6%	117.3%	115.0%

TABLE VIII
DYNAMIC PERFORMANCE OF CONVENTIONAL SRM WITH DIFFERENT TURN-OFF ANGLES $\theta_{on} = 0°$

Parameter	$\theta_{on} = 0°$				
	$\theta_{off} = 10°$	$\theta_{off} = 11°$	$\theta_{off} = 12°$	$\theta_{off} = 13°$	$\theta_{off} = 14°$
RMS phase current, A	3.638	4.254	5.029	5.909	6.856
Average torque, N·m	2.721	3.285	3.872	4.396	4.790
Torque per Ampere, N·m/A	0.748	0.758	0.770	0.744	0.699
Torque ripple	210.3%	189.7%	151.4%	122.0%	97.7%

is lower, but the superiority becomes smaller and smaller with the increase speed. This is because when the rate of change of flux linkage is high, as shown in (3) and (4), the dc-link voltage limits the rise of current. For the HESRM, owing to the effect of the PMs, the rate of change of flux linkage is higher than that in the conventional SRM, thus the superiority becomes smaller and smaller with the increase speed. For example, the average torque values produced by the HESRM at the low, medium, and high speeds are larger than those of the conventional SRM by 29.8%, 23.5%, 20.5%, and 18.0%. The torque ripple of the former is lower than those of the latter by 17%, 30%, 45.6%, and 15.6%. The output torque/power density of the former is larger than those of the latter by 42.1%, 35.2%, 32.7%, and 33.5% due to the light weight of the machine. Furthermore, the results indicate that the HESRM can generate a larger torque per ampere than the conventional SRM, while the copper loss and copper loss per torque of the former are lower than those of the latter.

C. *Effect of Excitation Angles*

As well known, excitation angles in SRMs can alter machine performance greatly. In order to investigate the effect of different turn-on and turn-off angles on the output performance of two SRM drives, the phase current and total torque waveforms under single-pulse control, varying the turn-on and turn-off angles, are simulated and shown in Fig. 23. In this study, the dc-link voltage and rotor speed are fixed. Each current and torque trace shown is for a different turn-off angle—from 10° to 14° with 1° intervals. Tables VI–VIII present detailed output performances of two SRM drives with different turn-on and turn-off angles. As shown

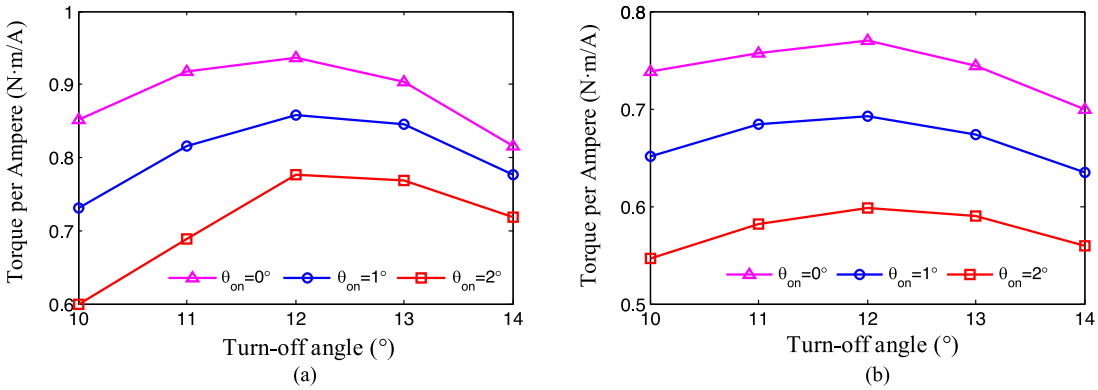

Fig. 24. Torque per ampere characteristics of two SRMs with different turn-on and turn-off angles. (a) Segmented HESRM. (b) Conventional SRM.

in these figures and tables, the root-mean-square (RMS) phase current and average torque of two SRM drives increase with the turn-off angle increases, whereas the torque ripple decreases with the turn-off angle increases. However, taking into account the torque per ampere characteristics, as shown in Fig. 24, the maximum torque per ampere is obtained with the turn-off angle of 12° in these two SRMs, which means that the coil current requirement under this operation condition is the lowest for the same torque. Thus, if considering the torque per ampere characteristics, the best turn-on and turn-off angles of two SRMs might be chosen as 0° and 12°, respectively.

D. Comparison With PM Flux-Switching Motor

For a better evaluation of the HESRM, it would be desirable to make a comparison with other PM motors, such as doubly salient PM motors and PM flux-switching motors. A comparison between the segmented HESRM and a PM flux-switching machine (PMFSM) is preliminarily performed based on FEA. To ensure a fair comparison, the two motors have the same basic dimensions as well as the electric steel material. Moreover, the wire gauge of the PMFSM is the same as that of the HESRM to keep the same conductivity and the slot fill factors of two motors are also kept the same. The main dimensions and parameters are listed in the following Table IX.

As shown in Table IX, the rotor iron weights are the same for both two motors. However, the stator iron ones are different. The stator of HESRM has 26.7% cost savings on steel compared to PMFSM. The entire machine weight of HESRM is lower than that of PMFSM by 7.8%. Furthermore, it can be seen that the usage of NdFeB in HESRM is much lower than that of PMFSM, which are 0.191 and 0.804 kg, respectively. Since the rare earth PM is very expensive than the iron lamination, the cost of the PMFSM will be much higher than the HESRM.

The open-circuit PM field distribution at the typical rotor position $\theta = 0^\circ$ and the transient field distribution when the phase-A is excited with a positive current in the PMFSM are shown in Fig. 25(a) and (b). Furthermore, the FEA results of phase currents and output torque with the same RMS phase current and rotor speed are compared with HESRM in Fig. 25(c)–(f). The detailed performances of two motors are shown in Table X. As can be seen, although the output torque of the PMFSM is larger than that of the HESRM, the torque and power densities of the two motors are almost the same. Thus, at this moment, it may be said that HESRM has values of power and torque density not too far from PMFSM of the same size as well as much lower cost.

TABLE IX
MAIN PARAMETERS AND SPECIFICATIONS OF THE HESRM AND PMFSM

Parameters	Segmented Stator HESRM	PMFSM
Phase number	3	3
Stator and rotor poles	12/10	12/10
Stator outer diameter (mm)	124	124
Stator- and rotor-pole arcs (°)	15/15	15/15
Stator yoke width (mm)	8.5	8.5
Rotor yoke width (mm)	10	10
Axial length (mm)	63	63
Air-gap length (mm)	0.3	0.4
Number of coil turns per pole	80	40
Winding weight (kg)	1.424	0.636
Stator iron weight (kg)	1.952	2.473
Rotor iron weight (kg)	0.858	0.858
Type of PM	NdFeB30	NdFeB30
PM weight (kg)	0.191	0.804
Total effective machine weight (kg)	4.425	4.771
Electric steel material	DW470	DW470

IV. EXPERIMENTAL VALIDATION

In order to validate above theoretical analysis and perditions, a 12/10 segmented-HESRM and a 12/10 conventional SRM with the same size are prototyped. The main dimensions and parameters of two SRMs are shown in Table I.

A. Motor Prototypes

Fig. 26 shows detailed photographs of the two SRM prototypes. The rotors of two SRMs have the same configuration which have ten salient poles and without any PMs or coils. The stator of the segmented HESRM is composed of six individual and modular U-shaped electrical steel laminated segments. Since the stator of the HESRM is not a monolithic entity as that in the conventional SRM, some special assembling technique and additional fixture/processing should be employed for supporting segmented stator, so this would add some construction

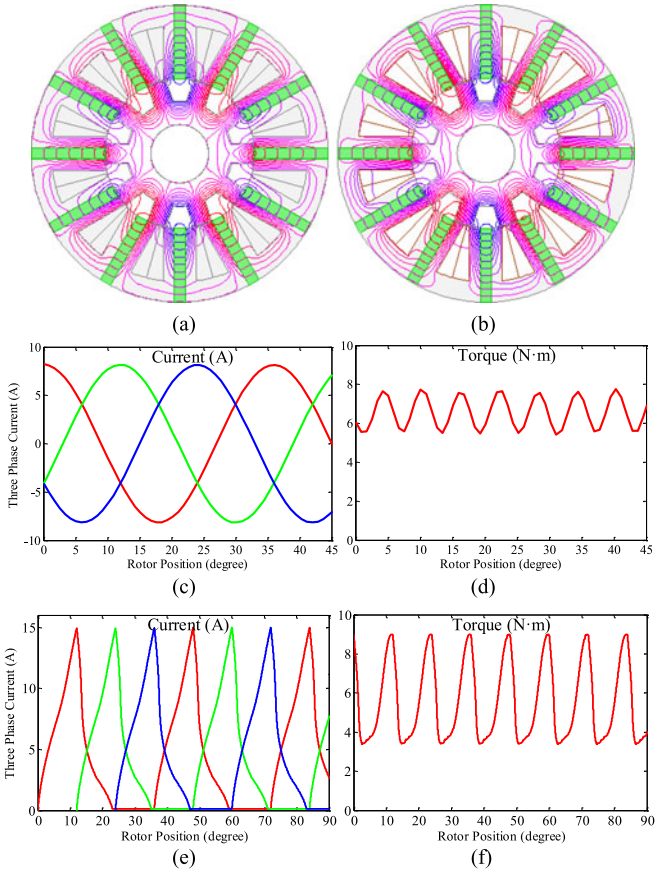

Fig. 25. Performance comparison of PMFSM and segmented HESRM. (a) Open-circuit PM field distribution of PMFSM. (b) Transient field distribution of PMFSM. (c) Transient phase currents of PMFSM. (d) Output torque of PMFSM. (e) Transient phase currents of HESRM. (f) Output torque of HESRM.

TABLE X
SUMMARY OF PREDICTED DYNAMIC PERFORMANCES OF TWO MOTORS

	PMFSM	Segmented HESRM
Speed, r/min	1200	1200
RMS phase current, A	5.85	5.85
Average torque, N·m	6.57	5.53
Torque ripple, %	33.2	101.3
Torque density, N·m/kg	1.38	1.25
Output power, W	825.1	694.6
Power density, W/kg	172.9	160.0
Torque per Ampere, N·m/A	1.12	0.99

cost. During the manufacture, each stator segment is placed in the inner side of a special sleeve-type fixture and fixed by two nonmagnetic metal bolts, as shown in Fig. 26(a). However, it should be noted that the cost of a sleeve fixture with sufficient stiffness is still cheaper than having a fully enclosed stator made of electrical steel. Two coils are wound on the poles of the segmented electromagnet core; afterward, the PM is installed on the indentation between two poles. Furthermore, it can be seen that both two SRMs have the same effective volume of complete motor assembly.

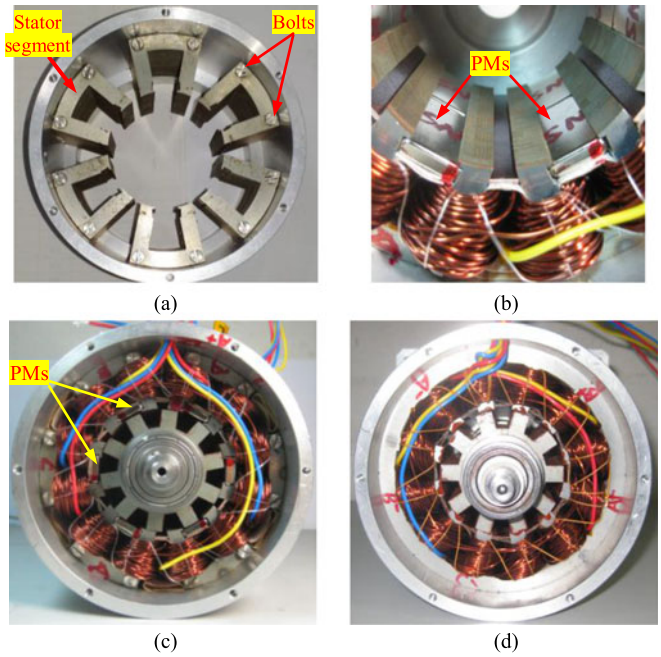

Fig. 26. Photographs of two SRM prototypes. (a) Segmented stator cores, (b) PMs and (c) motor assembly of the segmented HESRM. (d) Motor assembly of the conventional SRM.

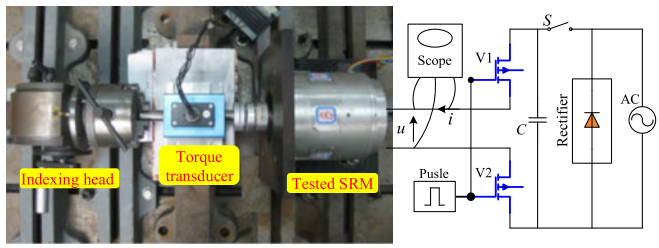

Fig. 27. Experimental setup for measuring static magnetic characteristics.

B. Static Flux Linkage and Torque Characteristics

A simple indirect method, which is called as capacitor-based pulse injection method, is performed to measure the static magnetic characteristics of two SRMs [38]. The experimental setup for measurement is shown in Fig. 27. The indexing head is utilized to lock the rotor at a certain position. An ac/dc converter is used to charge the capacitor, after that it was discharged to the phase winding through two Insulated Gate Bipolar Transistors (V1 and V2). Then, the flux linkage at a certain rotor position is estimated as follows:

$$\psi(\theta, i) = \int_0^t [u(t) - r \cdot i(t)]\, dt \Big|_{\theta=\text{const}} + \psi_0 \qquad (8)$$

where r is the winding resistance and ψ_0 is the initial flux linkage.

First, the measured flux linkages and FEA results with three current levels for two SRMs are shown in Fig. 28(a) and (b). It can be seen that FEA result and measured data agree well with each other. The maximum relative errors between FEA and measurement are about 3.2% and 3.6% for the HESRM and conventional SRM, respectively. Second, the measured static

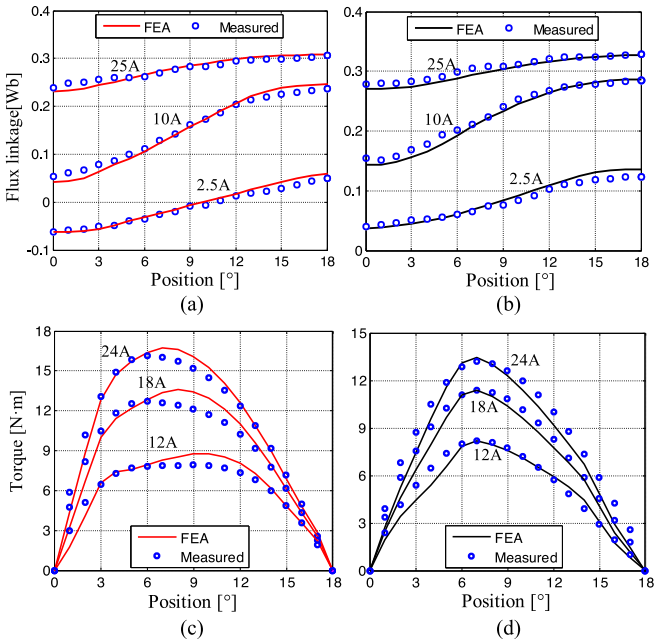

Fig. 28. FEA and measured static magnetic characteristics. (a) Flux linkage in the HESRM. (b) Flux linkage in the conventional SRM. (c) Static torque in the HESRM. (d) Static torque in the conventional SRM.

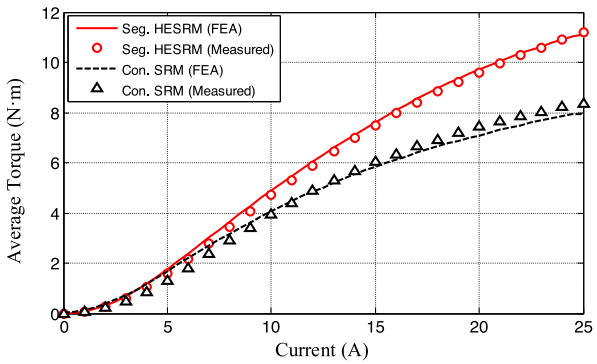

Fig. 29. Comparison of static average torque characteristics in two SRMs obtained from FEA and measurement.

torque and FEA results with three current levels for two SRMs are shown in Fig. 28(c) and (d). Accordingly, the FEA and measured average torque versus current characteristics for one half of electrical cycle in two SRMs are shown in Fig. 29. It is clear that higher average torque is obtained with the HESRM among large current range (>5 A) and good agreements are achieved between FEA and measurement. The maximum relative errors are about 2.5% and 3.8% for the HESRM and conventional SRM, respectively.

C. Steady-State Operation and Validation

The experimental setup for two SRM drives is shown in Fig. 30. It should be noted that the two SRMs are tested in one drive platform. The tested SRM is coupled with a hysteresis dynamometer as the loaded machine. An asymmetrical three-phase half bridge with its drive circuits is used as the power converter. A dSPACE 1104 acquisition system is used for developing control program and algorithm. Some other devices are also included in the experiment platform, such as voltage and current sensors, and encoder circuit.

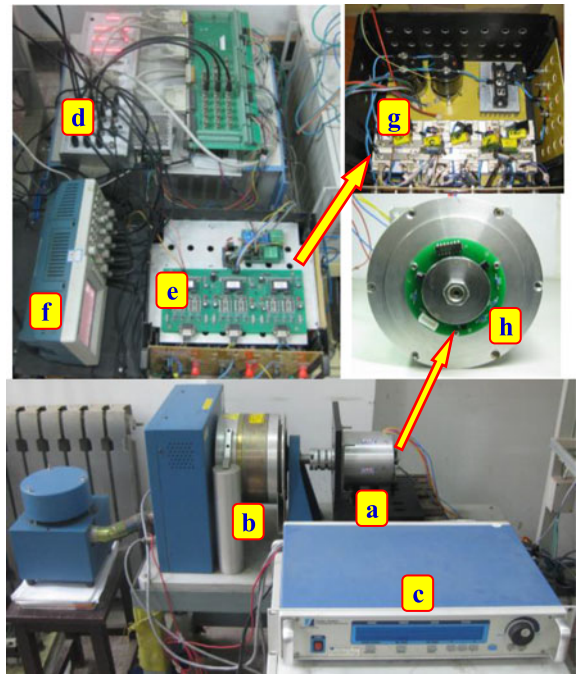

Fig. 30. Experimental platform for two SRM drives. (a) Tested SRM (segmented HESRM or conventional SRM). (b) Hysteresis dynamometer. (c) Dynamometer controller. (d) dSPACE. (e) Driving circuit. (f) Oscilloscope. (g) Power converter. (h) Encoder circuit.

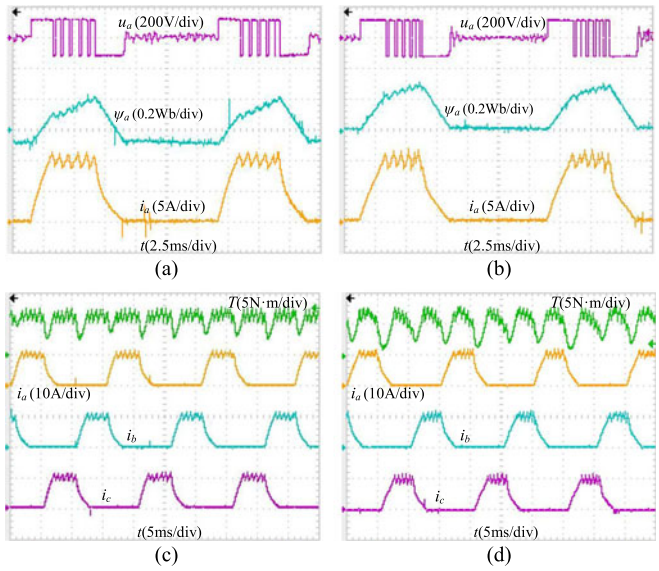

Fig. 31. Comparison of measured results of two SRMs under the same condition with CCC mode at 400 r/min. (a) and (c) HESRM. (b) and (d) Conventional SRM.

First, the steady-state operations of two SRMs with CCC mode under the same condition are tested and compared, as shown in Fig. 31. The dc-link voltage and speed are 140 V and

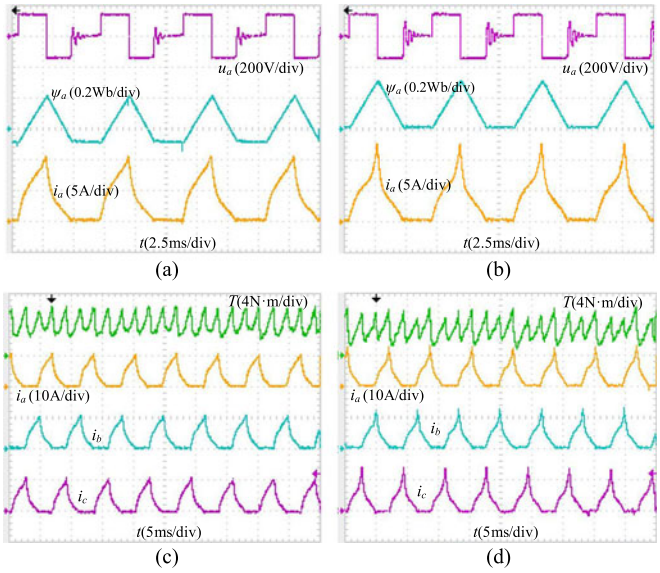

Fig. 32. Comparison of measured results of two SRMs under the same condition with APC mode at 900 r/min. (a) and (c) HESRM. (b) and (d) Conventional SRM.

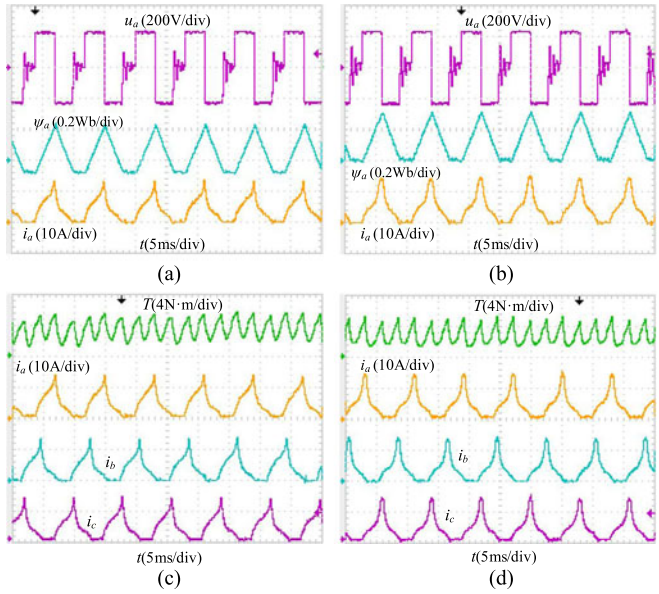

Fig. 33. Comparison of measured results of two SRMs under the same condition with APC mode at 1500 r/min. (a) and (c) HESRM. (b) and (d) Conventional SRM.

400 r/min, respectively. As expected, the HESRM produced higher average torque than the conventional SRM at this operation, which are 5.78 and 4.16 N·m, respectively. While the torque ripple of the former is lower than that of the latter by 25%. The phase flux linkage produced by the HESRM is also lower than that of the conventional SRM. Another comparison of two motors run at a medium speed of 900 r/min under APC mode with a dc-link voltage of 150 V is shown in Fig. 32. As expected, the segmented HESRM also produce higher average torque than the conventional SRM, which are 4.52 and 3.27 N·m, respectively. While the torque ripple and phase current of the former are also lower than those of the latter. It can be seen that the RMS current value of the HESRM is lower than that of the conventional SRM when they are operated with the same condition. As a result, the copper loss of the HESRM is doubtlessly lower and it indicates the HESRM can generate a larger torque per ampere. Furthermore, a comparison of two SRMs run at a high speed of 1500 r/min under APC mode with a dc-link voltage of 230 V as shown in Fig. 33. As expected, the HESRM also produce higher average torque than the conventional SRM, which are 4.01 and 3.38 N·m, respectively. While the torque ripple and phase current of the former are lower than those of the latter.

Second, the steady-state operation of two SRMs with APC mode is performed to validate the simulation. Fig. 34(a) compares the simulated and measured results of the HESRM operation at a dc-link voltage of 200 V and a speed of 1150 r/min. The turn-on and turn-off angles are 0° and 12°, respectively. Fig. 34(b) compares the simulation simulated and measured results of the conventional SRM operation at the dc-link voltage of 200 V and the speed of 1220 r/min. It can be seen that the simulation and experimental waveforms are in good agreement for two SRMs.

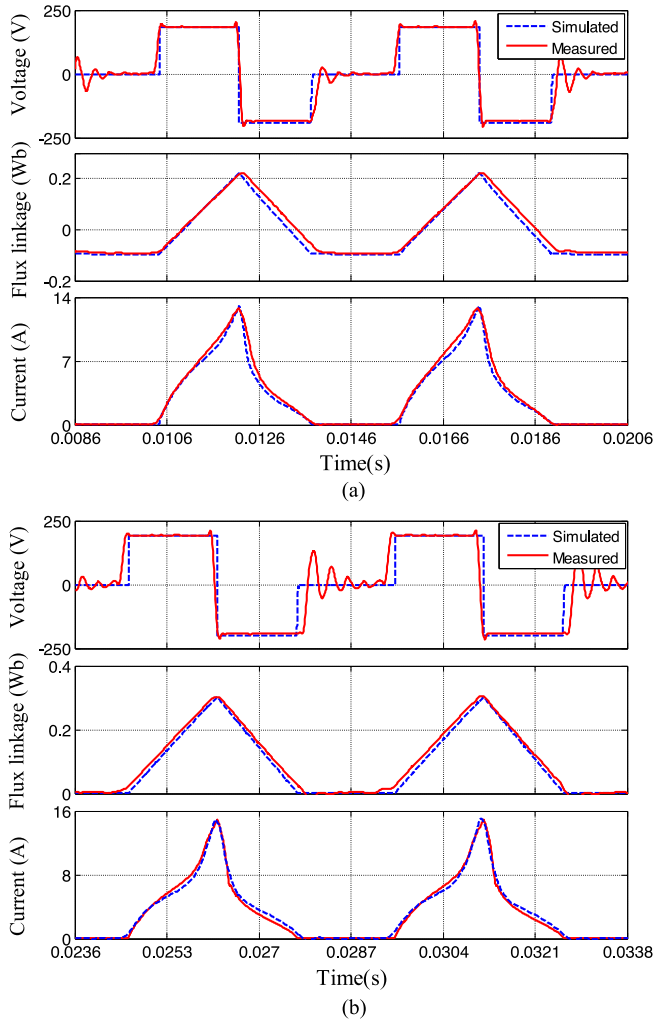

Fig. 34. Simulated and measured results of two SRMs with APC mode. (a) HESRM at 1150 r/min. (b) Conventional SRM at 1220 r/min.

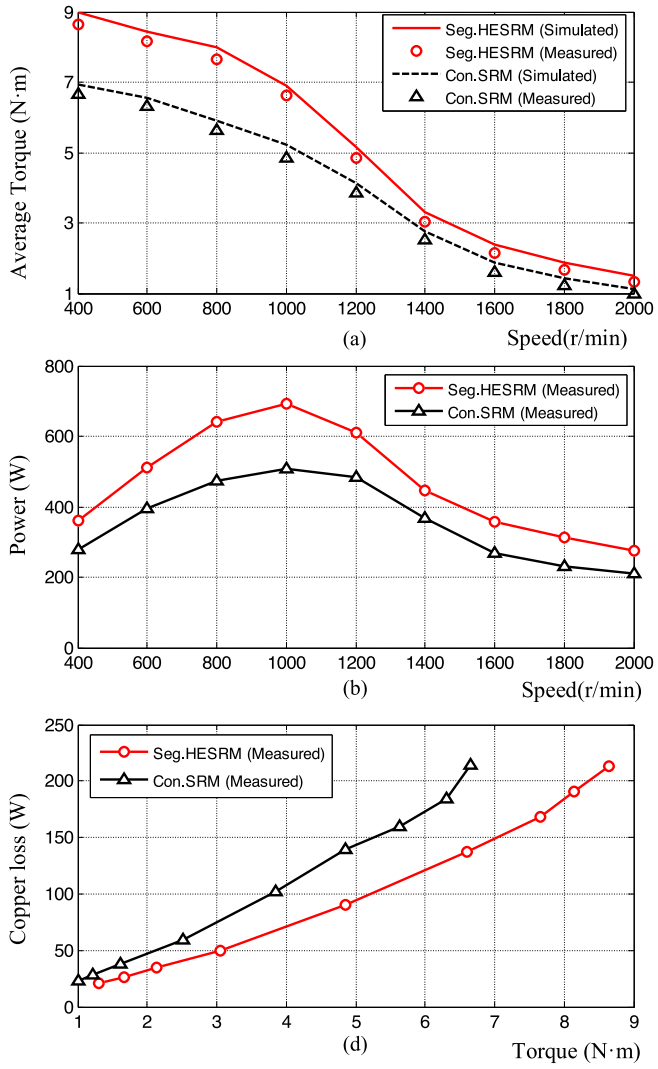

Fig. 35. Comparisons of (a) torque–speed, (b) power—speed, and (c) copper loss–torque characteristics of two SRMs.

Third, the average torque–speed, corresponding power–speed, and copper loss–torque characteristics of two SRMs under the same conditions are measured and validated, as shown in Fig. 35. In this study, both the two SRMs are fixed at the same dc-link voltage of 200 V and controlled with CCC mode (the CCC current is 14 A) at low-speed operation and APC mode (the turn-on and turn-off angles are 0° and 12°) at high-speed operation, respectively. The measured summary of comparative study between the two motor drives is shown in Table XI. As expected, the HESRM not only has wide range torque–speed characteristic, but also has higher average torque and higher output power with respect to conventional SRM under the same condition. For example, at the speed of 600 and 1200 r/min, the HESRM generates 30.1% and 20.5% larger torque/power than the conventional SRM. Consequently, the power and torque densities of the former are larger than those of the latter since the weight of the former is lower than the latter. The HESRM produces less copper loss than the conventional SRM for the same torque. As shown in Table XI, the copper loss of the HESRM is lower than

TABLE XI
MEASURED SUMMARY OF COMPARATIVE STUDY IN TWO SRMS

	Segmented HESRM			Conventional SRM		
Control modes	CCC	APC		CCC	APC	
Speed, r/min	600	1200	1800	600	1200	1800
RMS phase current, A	7.20	4.98	2.69	7.22	5.35	2.85
Average torque, N·m	8.21	4.85	1.66	6.31	3.86	1.28
Torque per Ampere, N·m/A	1.14	0.97	0.62	0.88	0.72	0.45
Output power, W	515.6	609.2	312.7	396.3	484.8	241.2
Output power density, W/kg	116.5	137.7	70.7	81.9	100.2	49.8
Copper loss, W	186.6	89.2	26.0	187.6	103.0	29.2
Copper loss per Torque, W/N·m	22.7	18.4	15.6	29.7	33.7	22.8
Efficiency, %	67.4	80.2	84.3	61.9	75.5	80.8

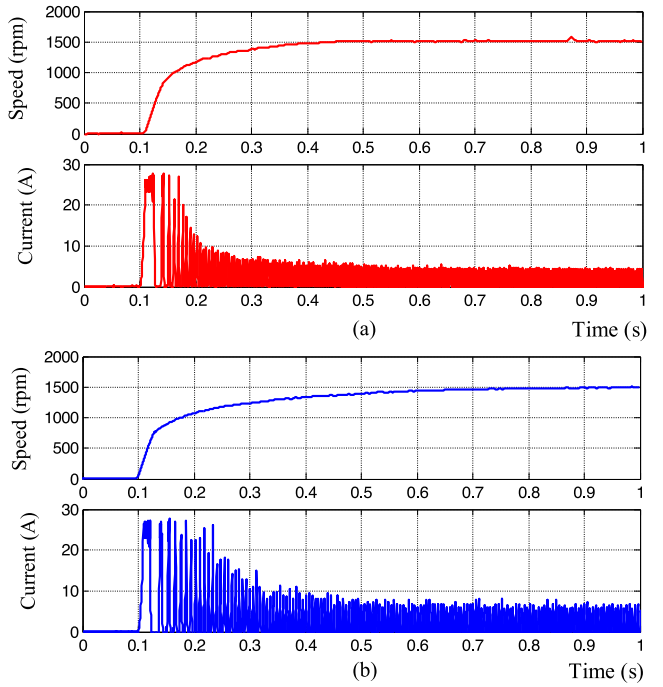

Fig. 36. Measured speed and phase current responses at start up under closed-loop control. (a) HESRM. (b) Conventional SRM.

that of the conventional SRM under the same speed operation. For example, the former produces 15.5% and 12.3% less copper loss than the latter at the same speed of 1200 and 1800 r/min, respectively. The HESRM also has higher torque per ampere and higher efficiency. The maximum achieved efficiency in the HESRM is about 84.3%, meanwhile is 80.8% in conventional SRM. The comparisons of dynamic characteristics validate the aforementioned analysis.

D. Transient Operation Validation

The transient start-up responses of the speed and phase current for two SRM drives with closed-loop control are tested and shown in Fig. 36. In this measurement, the two SRM drives are conducted under the same condition. The dc-link voltage is set at 150 V and the load torque is 1.5 N·m, respectively. During start up, these two SRMs are operated with CCC mode. It can be

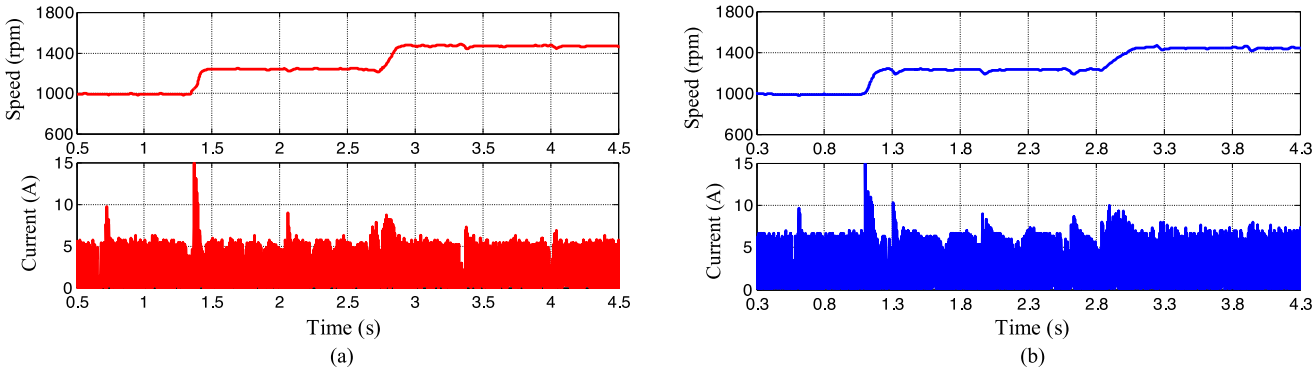

Fig. 37. Transient responses at step speed command changes 1000 → 1250 → 1500 r/min. (a) HESRM. (b) Conventional SRM.

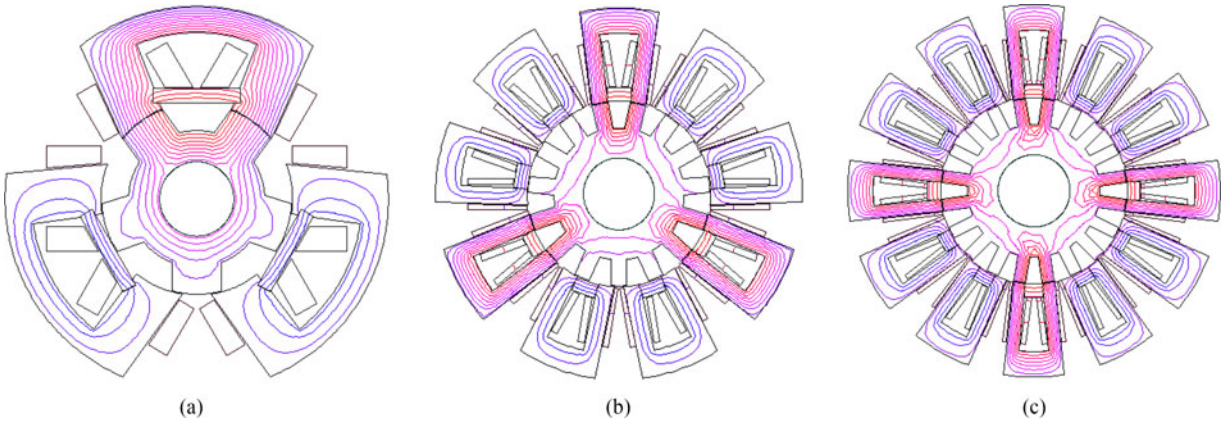

Fig. 38. Flux distributions of segmented HESRMs with different stator/rotor pole combinations in aligned position. (a) 6/5 pole. (b) 18/15 pole. (c) 24/20 pole.

found that the two SRMs both successfully perform self-startup and accelerate rapidly from standstill to the same commanded speed of 1500 r/min. However, the rotor speed of the HESRM rises faster than that of the conventional SRM. Thus, the rise-up time of the former is shorter than that of the latter, which are about 0.32 and 0.55 s, respectively. In other words, the HESRM has stronger starting capability than the conventional SRM. Furthermore, it is clear that the steady-state phase current of the HESRM is little lower than that of the conventional SRM.

Finally, the comparison of measured transient speed and corresponding phase current responses of two SRM drives at step speed command changes (1000 → 1250 → 1500 r/min) under the same condition, as shown in Fig. 37. The test results show that the rotor speeds of two SRMs can quickly track the command speed under closed-loop control and the speed ripples are very small. However, the regulated time of the HESRM is shorter than that of the conventional SRM.

E. Other Stator-/Rotor-Pole Combinations Machines

Apart from the 12/10 stator-/rotor-pole combination, there are several other combinations that could apply to this type of HESRMs, such as 6/5-, 18/15-, and 24/20-pole combinations, which are k times of 6/5 combination. The stator consists of N_S U-shaped segments; each one has two teeth and one PM. In other words, the number of stator segments N_S is equal to the number of PMs N_P, and the number of stator poles N_{SP} is two times of N_S. The least number of phases m is equal to the number of stator segments N_S. The rotor has N_R salient poles. The stator, with N_{SP} poles, is designed in such a way that, for each phase, there is a position of alignment of the stator poles with rotor poles and the stator segments with PMs have to be placed like Fig. 2(a). For a three-phase motor, the following rules should be considered:

$$N_S = N_P = 3k,\ N_{\mathrm{SP}} = 2N_S = 2N_P = 6k,$$
$$N_R = (2 \times 3 - 1) \cdot k = 5k. \tag{9}$$

The flux distributions of segmented HESRMs with different stator-/rotor-pole combinations in aligned position with one phase excited are shown in Fig. 38. It can be seen that the flux lines are symmetrically disposed in 18/15-pole and 24/20-pole machines. At this moment, the performance analysis and comparisons on these machines are currently in progress. This task will be the object of our future works and the simulation and experimental results will be presented in future paper.

VI. Conclusion

In this paper, a segmented-stator HESRM associated with PMs is comprehensively evaluated and quantitatively compared with a conventional SRM through FEA, modeling, and

experimental verification. The static magnetic characteristics, such as magnetic field line and flux density distribution, static flux linkage, and electromagnetic torque are evaluated and compared. The details of mathematical model and dynamic and transient performances of two SRMs are also presented and compared. From the comparative study, some conclusions are drawn as follows.

1) Although the segmented HESRM has six PMs in the stator, the entire effective machine mass is lighter than that of the conventional SRM by about 10%, which results in potential higher torque density.
2) When there is no current in the winding coils, the phase flux linkage due to the PM only in the segmented HESRM is -0.1 Wb at this situation. The phase flux linkage of the segmented HESRM is lower than that of the conventional one with the same current. The enclosed area of the flux linkage for segmented HESRM is larger than that for conventional SRM at a fixed current from unaligned to aligned positions, especially among large current range. The flux linkages created by the excited current and by the PMs in the segmented HESRM are strongly coupled.
3) In the large current range (>5 A), the segmented HESRM produces larger static torque than the conventional SRM. The static average torque of the segmented HESRM is 1.16 to 1.39 times higher than that of the conventional one for 8- to 25-A current.
4) The segmented HESRM also has better dynamic characteristics than the conventional SRM, such as higher average torque, lower torque ripple, larger power, and torque densities, etc. The average torque values produced by segmented HESRM at the low-, medium-, and high-speed operations are larger than those of conventional one by about 20%–30%. The output torque/power density of the segmented HESRM is larger than those of conventional one by approximately 30%–40% due to the light weight of the machine. The efficiency of segmented HESRM is higher than that of conventional one by approximately 3%–5%. The segmented HESRM has stronger starting capability than conventional SRM. The rotor speed of the former rises faster than that of the latter under the same condition and the regulated time of the former is also shorter. Thus, to some extent, for similar working condition and using the same motor size, it can be concluded that the segmented HESRM has higher torque/power capabilities as compared to the conventional SRM.

From the comprehensive evaluation and comparison, it can be concluded that the segmented HESRM would have a bright prospect in a wide of industrial applications with the requirements of higher torque/power capabilities, such as electric vehicle/hybrid electric vehicle applications.

REFERENCES

[1] M. Takeno, A. Chiba, N. Hoshi, S. Ogasawara, M. Takemoto, and M. A. Rahman, "Test results and torque improvement of the 50-kW switched reluctance motor designed for hybrid electric vehicles," *IEEE Trans. Ind. Appl.*, vol. 48, no. 4, pp. 1327–1334, Jul./Aug. 2012.

[2] V. Valdivia, R. Todd, F. J. Bryan, A. Barrado, A. Lázaro, and A. J. Forsyth, "Behavioral modeling of a switched reluctance generator for aircraft power systems," *IEEE Trans. Ind. Electron.*, vol. 61, no. 6, pp. 2690–2699, Jun. 2014.

[3] F. Yi and C. Wei, "Modeling, control, and seamless transition of the bidirectional battery-driven switched reluctance motor/generator drive based on integrated multiport power converter for electric vehicle applications," *IEEE Trans. Power. Electron*, vol. 31, no. 10, pp. 7099–7111, Oct. 2016.

[4] W. Ding, Y. F. Hu, and L. M. Wu, "Investigation and experimental test of fault-tolerant operation of a mutually coupled dual three-phase SRM drive under faulty conditions," *IEEE Trans. Power Electron.*, vol. 30, no. 12, pp. 6857–6872, Dec. 2015.

[5] W. Ding, "Comparative study on dual-channel switched reluctance generator performances under single- and dual-channel operation modes," *IEEE Trans. Energy Convers.*, vol. 27, no. 3, pp. 680–688, May 2012.

[6] J. Ye, B. Bilgin, and A. Emadi, "An extended-speed low-ripple torque control of switched reluctance motor drives," *IEEE Trans. Power Electron.*, vol. 30, no. 3, pp. 1457–1470, Mar. 2015.

[7] Y. Hu, C. Gan, W. P. Cao, and W. H. Li, "Central-tapped node linked modular fault-tolerance topology for SRM applications," *IEEE Trans. Power Electron.*, vol. 31, no. 2, pp. 1541–1554, Feb. 2015.

[8] Y. H. Hu, C. Gan, W. P. Cao, J. F. Zhang, W. H. Li, and S. J. Finney, "Flexible fault-tolerant topology for switched reluctance motor drives," *IEEE Trans. Power Electron.*, vol. 31, no. 6, pp. 4654–4668, Jun. 2016.

[9] S. H. Mao and M. C. Tsai, "A novel switched reluctance motor with C-core stators," *IEEE Trans. Magn.*, vol. 41, no. 12, pp. 4413–4420, Dec. 2005.

[10] X. D. Xue, K. W. E. Cheng, Y. J. Bao, P. L. Leung, and N. Cheung, "Switched reluctance generators with hybrid magnetic paths for wind power generation," *IEEE Trans. Magn.*, vol. 48, no. 11, pp. 3863–3867, Nov. 2012.

[11] L. Szabó and M. Ruba, "Segmental stator switched reluctance machine for safety-critical applications," *IEEE Trans. Ind. Appl.*, vol. 48, no. 6, pp. 2223–1229, Nov./Dec. 2012.

[12] M. Ruba, I. A. Viorel, and L. Szabó, "Modular stator switched reluctance motor for fault tolerant drive systems," *IET Electr. Power Appl.*, vol. 7, no. 3, pp. 159–169, Aug. 2013.

[13] A. Labak and N. C. Kar, "Designing and prototyping a novel five-phase pancake-shaped axial-flux SRM for electric vehicle application through dynamic FEA incorporating flux-tube modeling," *IEEE Trans. Ind. Appl.*, vol. 49, no. 3, pp. 1276–1288, May/Jun. 2013.

[14] C. Lee, R. Krishnan, and N. S. Lobo, "Novel two-phase switched reluctance machine using common-pole E-core structure: Concept, analysis, and experimental verification," *IEEE Trans. Ind. Appl.*, vol. 45, no. 2, pp. 703–711, Mar./Apr. 2009.

[15] C. Lee and R. Krishnan, "New designs of a two-phase E-core switched reluctance machine by optimizing the magnetic structure for a specific application: Concept, design, and analysis," *IEEE Trans. Ind. Appl.*, vol. 45, no. 5, pp. 1804–1814, Sep./Oct. 2009..

[16] B. C. Mecrow, E. A. El-Kharashi, J. W. Finch, and A. G. Jack, "Segmental rotor switched reluctance motors with single-tooth windings," *IEE Proc., Electr. Power Appl.*, vol. 150, no. 5, pp. 591–599, Sep. 2003.

[17] B. C. Mecrow, E. A. El-Kharashi, J. W. Finch, and A. G. Jack, "Preliminary performance evaluation of switched reluctance motors with segmental rotors," *IEEE Trans. Energy Convers.*, vol. 19, no. 4, pp. 679–686, Dec. 2004.

[18] J. D. Widmer and B. C. Mecrow, "Optimized segmental rotor switched reluctance machines with a greater number of rotor segments than stator slots," *IEEE Trans. Ind. Appl.*, vol. 49, no. 4, pp. 1491–1498, Jul./Aug. 2013.

[19] R. Vandana and B. G. Fernandes, "Design methodology for high performance segmented rotor switched reluctance motors," *IEEE Trans. Energy Convers.*, vol. 30, no. 1, pp. 11–21, Mar. 2015.

[20] Z. Y. Xu, D. H. Lee, and J. W. Ahn, "Design of a novel 6/5 segmental rotor type switched reluctance motor," in *Proc. Ind. Appl. Soc. Annu. Meet.*, 2014, pp. 1–7.

[21] H. T. Zhang, F. G. Zhang, D. H. Lee, and J. W. Ahn, "Design and performance analysis of segmental rotor type 12/8 switched reluctance motor," in *Proc. Int. Conf. Expo. Transp. Electr. Asia-Pac.*, 2014, pp. 1–6.

[22] X. Y. Chen, Z. Q. Deng, X. L. Wang, J. J. Peng, and X. S. Li, "New designs of switched reluctance motors with segmental rotors," in *Proc. IET Int. Conf. Power Electron. Mach. Drives*, 2010, pp. 1–6.

[23] J. D. Widmer, R. Martin, and B. C. Mecrow, "Optimisation of an 80kW segmental rotor switched reluctance machine for automotive traction," *IEEE Trans. Ind. Appl.*, vol. 51, no. 4, pp. 2990–2999, Jul./Aug. 2015.

[24] W. Ding, Y. F. Hu, and L. M. Wu, "Analysis and development of novel three-phase hybrid magnetic path switched reluctance motors using modular and segmental structures for EV applications," *IEEE/ASME Trans. Mechatronics*, vol. 20, no. 5, pp. 2437–2451, Oct. 2015.
[25] W. Ding, G. Z. Ying, L. Liu, and J. Y. Lou, "Magnetic circuit model and finite-element analysis of a modular switched reluctance machine with E-core stators and multi-layer common rotors," *IET Electr. Power Appl.*, vol. 8, no. 8, pp. 296–309, Aug. 2014.
[26] Y. Hasegawa, K. Nakamura, and O. Ichinokura, "A novel switched reluctance motor with the auxiliary windings and permanent magnets," *IEEE Trans. Magn.*, vol. 48, no. 11, pp. 5574–5589, Nov. 2012.
[27] K. Nakamura and O. Ichinokura, "Super-multipolar permanent magnet reluctance generator designed for small-scale wind-turbine generation," *IEEE Trans. Magn.*, vol. 48, no. 11, pp. 3311–3314, Nov. 2012.
[28] E. Sunan, F. Kucuk, H. Goto, H. J. Guo, and O. Ichinokura, "Three-phase full-bridge converter controlled permanent magnet reluctance generator for small-scale wind energy conversion systems," *IEEE Trans. Energy Convers.*, vol. 29, no. 3, pp. 583–593, Sep. 2014.
[29] K. Y. Lu, P. O. Rasmussen, S. J. Watkins, and F. Blaabjerg, "A new low-cost hybrid switched reluctance motor for adjustable-speed pump applications," *IEEE Trans. Ind. Appl.*, vol. 47, no. 1, pp. 314–321, Jan./Feb. 2011.
[30] K. Y. Lu, U. Jakobsen, and P. O. Rasmussen, "Single-phase hybrid switched reluctance motor for low-power low-cost applications," *IEEE Trans. Magn.*, vol. 47, no. 10, pp. 3288–3291, Oct. 2011.
[31] U. Jakobsen, K. Y. Lu, P. O. Rasmussen, and D. H. Lee, "Sensorless control of low-cost single-phase hybrid switched reluctance motor drive," *IEEE Trans. Ind. Appl.*, vol. 51, no. 3, pp. 2381–2387, May/Jun. 2015.
[32] P. Andrada, B. Blanqué, E. Martínez, and M. Torrent, "A novel type of hybrid reluctance motor drive," *IEEE Trans. Ind. Electron.*, vol. 61, no. 8, pp. 4337–4345, Aug. 2014.
[33] K. Nakamura, E. Sunan, and O. Ichinokura, "Development of 72/96-pole rare-earth free permanent magnet reluctance generator for small-scale renewable power generation," *IEEJ J. Ind. Appl.*, vol. 3, no. 1, pp. 41–46, 2015.
[34] S. K. Liu, J. H. Du, and D. L. Liang, "Modeling of double-rotor permanent magnet reluctance motor," in *Proc. 17th Int. Conf. Electr. Mach. Syst.*, 2014, pp. 1587–1590.
[35] W. Ding, Y. F. Hu, H. G. Fu, and Q. S. Chen, "Evaluation of a segmented stator hybrid excitation switched reluctance machine with permanent magnets for electric vehicles," in *Proc. 11th Int. Conf. Ecolog. Veh. Renewable Energies*, 2016, pp. 1–8.
[36] R. Krishnan, A. S. Bharadwaj, and P. N. Materu, "Computer aided design of electrical machines for variable speed applications," *IEEE Trans. Ind. Electron.*, vol. 36, no. 4, pp. 560–571, Nov. 1988.
[37] R. Y. Tang, *Modern Permanent Magnet Machines: Theory and Design*. Beijing, China: China Machine Press, 2000.
[38] S. J. Song, M. Zhang, and L. F. Ge, "A new fast method for obtaining flux-linkage characteristics of SRM," *IEEE Trans. Ind. Electron.*, vol. 62, no. 7, pp. 4105–4117, Jul. 2015.

Wen Ding (M'11) received the B.S. degree from the Xi'an University of Technology, Xi'an, China, in 2003, and the M.S. and Ph.D. degrees from Xi'an Jiao tong University, Xi'an, in 2006 and 2009, respectively, all in electrical engineering.

He is currently an Associate Professor with the School of Electrical Engineering, Xi'an Jiaotong University. His research interests include electrical machines and drives with emphasis on switched reluctance machine design and control, electric vehicles and hybrid electric vehicles, aerospace starter/generator, industrial applications of electromagnetic devices.

Haigang Fu received the B.S. degree in electrical engineering from Xi'an Jiaotong University, Xi'an, China, in 2014. He is currently working toward the M.S. degree still in electrical engineering from Xi'an Jiaotong University, Xi'an, China.

His research interests include motor design, motor drives and control with emphasis on hybrid excitation switched reluctance motor.

Yanfang Hu received the B.S. and M.S degree in 2011 and 2015, respectively. She is currently working toward the Ph.D. degree at the School of Electrical Engineering, Xi'an Jiaotong University, Xi'an, China.

Her research interests include electrical machines and drives with emphasis on switched reluctance machine design and control.